

Two-Dimensional Numerical Simulation of O-mode to Z-mode Conversion in the Ionosphere

P. D. Cannon,¹ F. Honary,¹ N. Borisov,²

¹Space and Planetary Physics (SPP) Group, Department of Physics, Lancaster University, Lancaster, UK.

²Institute of Terrestrial Magnetism, Ionosphere and Radio Waves Propagation (IZMIRAN), 142190 Troitsk, Russia.

Published in *Journal of Geophysical Research: Space Physics*, 121(3), 2755-2782, doi:10.1002/2015JA022105

Key Points:

- 2D numerical simulation of O- to Z-mode wave conversion during ionospheric modification
- Angular shape of conversion window influenced by background electron density profile
- Plasma temperature and density perturbation dependent on incident pump wave direction

Abstract

Experiments in the illumination of the F-Region of the ionosphere via radio-frequency waves polarized in the ordinary mode (O-mode) have revealed that the magnitude of artificial heating-induced effects depends strongly on the inclination angle of the pump beam, with a greater modification to the plasma observed when the heating beam is directed close to or along the magnetic zenith direction. Numerical simulations performed using a recently developed Finite-Difference Time-Domain (FDTD) code are used to investigate the contribution of the O-mode to Z-mode conversion process to this effect. The aspect angle dependence and angular size of the radio window for which conversion of an O-mode pump wave to the Z-mode occurs is simulated for a variety of plasma density profiles including 2D linear gradients representative of large-scale plasma depletions, density-depleted plasma ducts and periodic field-aligned irregularities. The angular shape of the conversion window is found to be strongly influenced by the background plasma profile. If the Z-mode wave is reflected, it can propagate back towards the O-mode reflection region leading to resonant enhancement of the electric field in this region. Simulation results presented in this paper demonstrate that this process can make a significant contribution to the magnitude of electron density depletion and temperature enhancement around the resonance height, and contributes to a strong dependence of the magnitude of plasma perturbation with the direction of the pump wave.

1. Introduction

The use of high-power radio-frequency (RF) transmitters to perturb the Earth's ionosphere gives a unique opportunity to study the complex and often non-linear mechanisms that underpin the interaction between an electromagnetic (EM) wave and ionospheric plasma. The ionosphere can be treated as a vast plasma laboratory, in which experiments can be performed without the limited spatial scale-size and chamber edge effects one may encounter while performing plasma experiments in a laboratory. Experiments in the illumination of the F-Region of the ionosphere via RF waves polarized in the ordinary mode (O-mode) have resulted in the observation of a wide range of non-linear thermal phenomena associated with the excitation of plasma waves and instabilities [Robinson, 1989; Rietveld *et al.*, 2003]. Many of these processes can induce significant enhancements of the electron temperature around the region in which the EM wave most strongly interacts with the plasma [Gordon and Carlson, 1974; Meltz *et al.*, 1974; Djuth *et al.*, 1987; Stocker *et al.*, 1992; Honary *et al.*, 1993]. Substantial changes to the electron density have also been commonly observed on a variety of different spatial scales, from large-scale density depletions spanning several kilometres [Gurevich *et al.*, 2002] to small-scale irregularities aligned with the geomagnetic field and having transverse scale sizes ranging from a few metres down to a few centimetres, as detected by rockets and VHF-UHF backscattering [Kelley *et al.*, 1995].

The main processes driving the enhancement of electron temperature in ionospheric modification experiments involve the excitation of large-amplitude plasma waves below the O-mode reflection height where the frequency of the incident pump wave is close to the local upper-hybrid (UH) wave frequency. In this region, provided that the pump frequency is not close to an electron gyroharmonic [Rao and Kawp, 1990; Stubbe *et al.*, 1994], electrostatic (ES) UH waves propagating in a direction perpendicular to the geomagnetic field are readily excited [Wong *et al.*, 1981; Dysthe *et al.*, 1982; Antani *et al.*, 1996]. ES waves of this nature induce the formation of striations in the electron density profile, elongated along the magnetic field direction and with a comparatively small transverse scale size. The region of interaction is initially narrow, but broadens as the striations grow with

time. In the stationary state, the vertical scale of this region is several kilometres [Borisov and Robinson, 2003]. Explosive heating of electron gas local to the striations then proceeds via the nonlinear resonance instability [Gurevich et al., 1995, 2001; Gondarenko et al., 2005], as incident pump wave electric field becomes trapped in the density depletions and amplified through efficient excitation of further UH modes. Collisional damping of the trapped waves is highly efficient within the striations and leads to an increase in the local plasma temperature, and consequently to a increase in the electron density depletion within the irregularities. As the striations deepen, the efficiency of trapping increases, and leads to a rapid, nonlinear increase in the electron temperature around the UH resonance height.

The formation of small-scale density irregularities reduces the average electron plasma density around the UH resonance region and leads to a focusing of the pump wave and thus to a further enhancement of the E-field amplitude in this region [Gurevich et al., 2001; Gondarenko et al., 2003]. Self-focusing of this nature results in further nonlinear enhancement of the electron temperature and causes the evolution of a hierarchy of density-depleted structures around the O-mode reflection height, from the small-transverse-scale (1-10s of metres) striations associated with the resonance (thermal parametric) instability to self-organized bunches of striations forming duct-like density depleted structures due to the self-focusing instability spanning up to many kilometres in transverse scale [Gurevich et al., 1998]. Close-packed duct-like structures of this nature are known to form large-scale semi-permanent density-depleted regions or duct-like channels which may affect wave propagation.

Observations have revealed that the magnitude of such artificial heating-induced perturbations to the plasma density depends strongly on the inclination angle of the RF pump beam, with a greater modification to the plasma observed when the heating beam is directed away from the vertical direction towards the magnetic zenith, as reported, for example, by [Honary et al., 2011; Kosch et al., 2000; Pedersen et al., 2003]. This magnetic zenith effect has been observed as an increase in electron temperature enhancement by a factor of 2 or greater compared to off-zenith operation [Rietveld et al., 2003; Dhillon and Robinson, 2005], and has also been seen to correspond to a greater enhancement in the characteristic ion and electron plasma lines seen in UHF incoherent scatter radar spectra and an increase in the backscatter power due to field-aligned irregularities.

To explain theoretically the unexpected electron temperature and optical emission enhancements arising due to heating directed along the magnetic zenith direction, the self-focusing instability was first suggested as the mechanism behind this effect [Gurevich et al., 2002; Gurevich et al., 2005]. The timescale for this process to manifest is known to be long (of the order of 1min). The experiments recently performed by [Honary et al., 2011] demonstrated that the rise of electron temperature occurs on a much more rapid timescale (of the order of a few seconds; comparative to the rise time of field-aligned striations). Instead, [Honary et al., 2011] proposed that this aspect-angle dependence of heating is in part due to the O-mode to Z-mode (slow branch of the extraordinary mode) conversion process that can occur in the F-region of the ionosphere for a narrow window of pump wave inclination angles. The Z-mode is able to penetrate to altitudes above the O-mode reflection height, where the conversion of EM waves trapped in field-aligned irregularities to plasma modes is more efficient. This leads to a more rapid development of the resonance instability and potentially a greater magnitude of electron temperature enhancement.

To fully understand the fundamental wave interaction process involved in the O-mode to Z-mode conversion process, it is useful to augment experimental findings with accurate numerical simulations. Ionospheric plasma processes have previously benefited from investigation using full-wave numerical simulation codes, for example as reported by [Gondarenko et al., 2003] who used an alternating-direction implicit (ADI) model to simulate linear mode conversion processes, [Eliasson and Stenflo, 2008] who studied the parametric decay instability and the generation of Langmuir turbulence around the interaction height using a generalized Zakharov model, or [Leyser and Nordblad, 2009; Nordblad and Leyser, 2010] who simulated the Z-mode pumping of a non-linear density ducts such as that formed via the self-focusing instability using ray tracing coupled with a Runge-Kutta scheme. In this paper, a recently developed full-wave FDTD code [Cannon and Honary, 2015] is used to study this conversion process in two spatial dimensions, allowing the variety of background density scenarios to be investigated. Time-dependent on-grid updates to the plasma density and temperature included in the FDTD algorithm meant that the impact of O- to Z-mode conversion on the growth of thermal-scale plasma perturbations could be simulated.

The paper is structured as follows. In Section 2, the numerical simulation algorithm is introduced. In Section 3 the simulation code is used to calculate the radio window for which conversion from O-mode to Z-mode is favourable for a simplified linear density gradient, with the results shown to be in good agreement with the theoretical predictions of [Mjølhus, 1984]. The code is then used to demonstrate how the radio window is modified by the presence of plasma density features of varying scale sizes, such as density-depleted ducts or striations. Section 4 presents the results of full-wave plasma simulations demonstrating that the excitation and subsequent reflection of the Z-mode wave has a strong influence on the magnitude of heating-induced effects such as temperature enhancement developed around the interaction region. Simulations of plasma heating experiments for a range of pump wave launch angles show that the O-mode to Z-mode conversion process is a key mechanism contributing

to the observed magnetic zenith effect. In Section 5 the effects of adding density-depleted plasma irregularities are investigated, with the influence of this process on the enhancement of electron temperature demonstrated to be heavily dependent on both pump wave inclination angle and irregularity characteristics.

2. Methodology

To numerically simulate an ionospheric modification experiment, this study uses the GPU-accelerated FDTD code described and validated in [Cannon and Honary, 2015]. The FDTD method, first proposed in [Yee, 1966], has an advantage over many other numerical simulation techniques as it deals with complex, nonlinear and impulsive interactions in a natural and time-explicit manner, avoiding complex and computationally-intensive linear algebra calculations. FDTD is a particularly useful tool for geophysical modelling due to the fact that the grid-based structure allows medium properties such as plasma density or temperature to be defined separately at each point. The algorithm used here assumes a multi-fluid description of a dynamic, anisotropic, collisional plasma, in which electron or charged ion species are treated as individual fluids of continuous mass and charge. The effect on wave propagation due to the presence of plasma is introduced through the coupling of Maxwell's wave equations with the Lorentz equations of motion for each constituent plasma species, with anisotropy introduced through inclusion of a static externally-applied magnetic field in a manner similar to that described by [Young, 1994] or [Yu and Simpson, 2010]. The time-dependent variation of plasma temperature and density are treated by the inclusion of expressions for the dynamic behaviors of small perturbations of the plasma fluid temperature and density [Gurevich, 1978]. Together, these form a set of coupled first-order partial differential equations which govern the time dependent behavior of the EM wave and plasma medium:

$$\nabla \times \mathbf{E} = -\mu_0 \frac{\partial \mathbf{H}}{\partial t} \quad (1)$$

$$\nabla \times \mathbf{H} - \sum_a N_a e_a \mathbf{U}_a = \varepsilon_0 \frac{\partial \mathbf{E}}{\partial t} \quad (2)$$

$$N_a m_a \frac{\partial \mathbf{U}_a}{\partial t} = N_a e_a (\mathbf{E} + \mathbf{U}_a \times \mathbf{B}) - N_a m_a \nu_a \mathbf{U}_a - \nabla (k_B N_a T_a) \quad (3)$$

$$\frac{\partial N_a}{\partial t} + \nabla \cdot (N_a \mathbf{U}_a) = 0 \quad (4)$$

$$\frac{3}{2} k_B \frac{\partial}{\partial t} (N_a T_a) + \nabla \cdot \mathbf{Q}_a - N_a e_a \mathbf{E} \cdot \mathbf{U}_a - \Delta \varepsilon_a = 0 \quad (5)$$

In these expressions, subscript a refers to plasma component species. \mathbf{U} is the time-varying fluid bulk velocity vector, $\mathbf{B} = B \hat{\mathbf{b}}$ is the static background magnetic field, T and N are the plasma temperature and number density respectively, $\nabla \cdot \mathbf{Q}$ describes the heat flux transport, $\Delta \varepsilon$ is a collisional heating term, e_a and m_a refer to particle charge and mass respectively, ε_0 and μ_0 are the permittivity and permeability of free space respectively, and k_B is the Boltzmann constant. ν represents the effective collision frequency given by Equation (6) [Gondarenko et al., 2005]:

$$\nu(N, T) = \nu_0 \left(\frac{N}{N_0} \right) \left(\frac{T}{T_0} \right)^{-3/2} \quad (6)$$

where ν_0 , N_0 and T_0 are the unperturbed effective collision frequency, number density and temperature respectively. The effective collision frequency incorporates both collisions with other plasma particles and with the neutral background species, such that $\nu_e = \nu_{ei} + \nu_{en}$ and $\nu_i = \nu_{ie} + \nu_{in}$, where ν_{ei} , ν_{ie} , ν_{en} and ν_{in} are the electron-ion, ion-electron, electron-neutral and ion-neutral collision frequencies respectively. In the simulation studies described below, the undisturbed collision frequencies ν_0 were chosen to represent typical conditions in the F-region at Tromsø, and updated every time-step via (6) to reflect simulated perturbations to the plasma medium. Simulated fields are updated sequentially via a leapfrog time-stepping scheme, following the cyclical update pattern: $\mathbf{E}^q \rightarrow T^q \rightarrow \mathbf{H}^{q+\frac{1}{2}} \rightarrow \mathbf{U}^{q+\frac{1}{2}} \rightarrow N^{q+1} \rightarrow \mathbf{E}^{q+1} \rightarrow \dots$ Here \mathbf{E} , \mathbf{H} , \mathbf{U} , T and N represent the simulated electric field, magnetic field, fluid velocity, plasma temperature and density respectively. The index q refers to the simulation time step number. The inclusion in the time-stepping algorithm of on-grid updates to perturbations of the plasma medium allows non-linear plasma processes such as the resonance instability or self-focusing instability to develop naturally in the simulation volume.

3. Numerical Simulation of Radio Window

A vital process in understanding the Magnetic Zenith Effect is thought to be the transition from O-mode polarized pump wave to a Z-mode (slow-branch X-mode) wave that may occur as the pump wave approaches the interaction height [Mjølhus and Flå, 1984; Mjølhus, 1990]. This process is highly dependent on the initial inclination angle of the pump wave with respect to the direction of the geomagnetic field near the O-mode reflection point. Conditions most favourable for conversion to Z-mode occur when the \mathbf{k} -vector of the incident wave is close to being parallel to the geomagnetic field direction at the height at which the transformation takes place ($\omega_{pe} = \omega_0$, where ω_0 is the frequency of the pump wave). This condition corresponds to the L-mode wave near the $k_{\perp} = 0$ limit of the O-mode dispersion surface; this wave is able to continue beyond $\omega_{pe} = \omega_0$ on the Z-mode branch of the X-mode dispersion surface [Leyser and Nordblad, 2009]. The angular dependence leads to the formation of a "radio window" as described in, for example, [Mjølhus, 1984]: a range of inclination angles for which the pump wave is partially or fully transmitted beyond the O-mode reflection height as a Z-mode wave. As the direction of the incident wave \mathbf{k} -vector is governed by the refractive properties of the local plasma the wave passes through, the spatial profile of ionospheric plasma around the interaction height has a significant influence on the angular position and characteristics of the radio window, and thus on the development of the magnetic zenith effect. A strength of a full-wave numerical code such as that described in Section 2 is that it allows wave propagation through plasma to be accurately computed in scenarios for which analytical evaluation may be impossible without resorting to constraining regimes of approximation, for example those employed by geometric optics or similar [Budden, 1961; Ginzburg, 1970]. The FDTD scheme used here automatically incorporates linear mode conversion processes such as the O-mode to Z-mode transition into the time-domain evolution of the simulated EM fields and the coupled on-grid updates to plasma density and temperature perturbation mean that the time-dependent and nonlinear plasma response to an incident wave is directly included in any calculation. This Section presents the results of a series of simulations run using the FDTD code described in Section 2 to investigate the effect of different plasma density profiles on the characteristics of the ionospheric radio window.

The simulation was set up as a two-dimensional scenario, with all wave propagation restricted to lie in the xz -plane, and all medium properties assumed to be homogeneous in the y -direction. A computational domain of dimensions $1280 \times 1 \times 1280$ Yee cells [Yee, 1966] was used, with the discrete spatial step size (Δ_x) set as $5.50 m$ in all directions. To ensure numerical stability the Courant number [Taftove and Hagness, 2000] was chosen to be 0.5, which fixed the size of the discrete time step (Δ_t) to be $9.17 \times 10^{-9} s$. The simulation was terminated on all sides by a 32-cell complex-frequency-shifted perfectly-matched layer (CFS-PML) designed to ensure that any waves leaving the domain were absorbed with the minimum possible numerical reflection [Berenger, 1994]. For the plasma temperature and density, edge termination was achieved using a Neumann boundary condition that set the gradient of each to zero along the direction of the background magnetic field. A wave launching layer based on the principles of the total-field scattered-field implementation described in [Schneider, 2004] was used to introduce continuous electromagnetic waves of O-mode polarization into the domain to represent the heating pump wave. The wave frequency was chosen to be $\omega_0 = 2\pi \times 4.54 MHz$. Background plasma parameters were chosen to represent typical F-region conditions during a heating experiment at Tromsø. Typical plasma parameters were obtained using IRI-2012 [Bilitza et al., 2014]. An idealized ionospheric plasma was represented by a 1D linear vertical electron density profile of the form (7).

$$N_0(z) = N_{crit} \left(1 + \frac{z - z_{crit}}{L_z} \right) \quad (7)$$

In this expression, N_{crit} is the electron density at $X = \frac{\omega_{pe}^2}{\omega_0^2} = 1$, where ω_{pe} is the fundamental plasma frequency for electrons. z_{crit} is the distance above the lower edge of the simulation at which the critical density occurs, here set to be $4.11 km$ above the $z = 0$ plane. L_z is the scale height of the density gradient, set to be $20 km$. The background electron temperature was set to be $1800 K$. A population of ions of average mass $16 AMU$ (representing O^+ ions) was included with a background density distribution equivalent to that of the electrons to preserve neutrality, and an initialized temperature of $900 K$. The unperturbed collision frequencies for electrons and ions were set to be $500 s^{-1}$ and $6 s^{-1}$ respectively. A static magnetic field of magnitude $|\mathbf{B}| = 4.16 \times 10^{-5} T$ was initialized in the domain at an angle of $\alpha = 12^\circ$ to the vertical. This was set to be uniform throughout the simulation domain, hence resulting in electron and ion gyrofrequencies of $\omega_{ce} = 2\pi \times 1.17 MHz$ and $\omega_{ci} = 2\pi \times 39.7 Hz$ respectively.

To investigate the angular characteristics of the O-to-Z-mode conversion process, a set of simulations were performed with the launch angle of the pump wave with respect to the vertical direction, θ , varied from $\theta = 0^\circ$ (pump wave \mathbf{k} -vector directed vertically, and in this case along the direction of the electron density gradient) to $\theta = 12^\circ$ (pump wave \mathbf{k} -vector along the direction of the simulated geomagnetic field) in $\Delta\theta = 0.01 rad$ (0.57°) steps. The simulations were run for 1×10^5 time steps (equivalent to $9.17 \times 10^{-4} s$), which was a sufficiently long

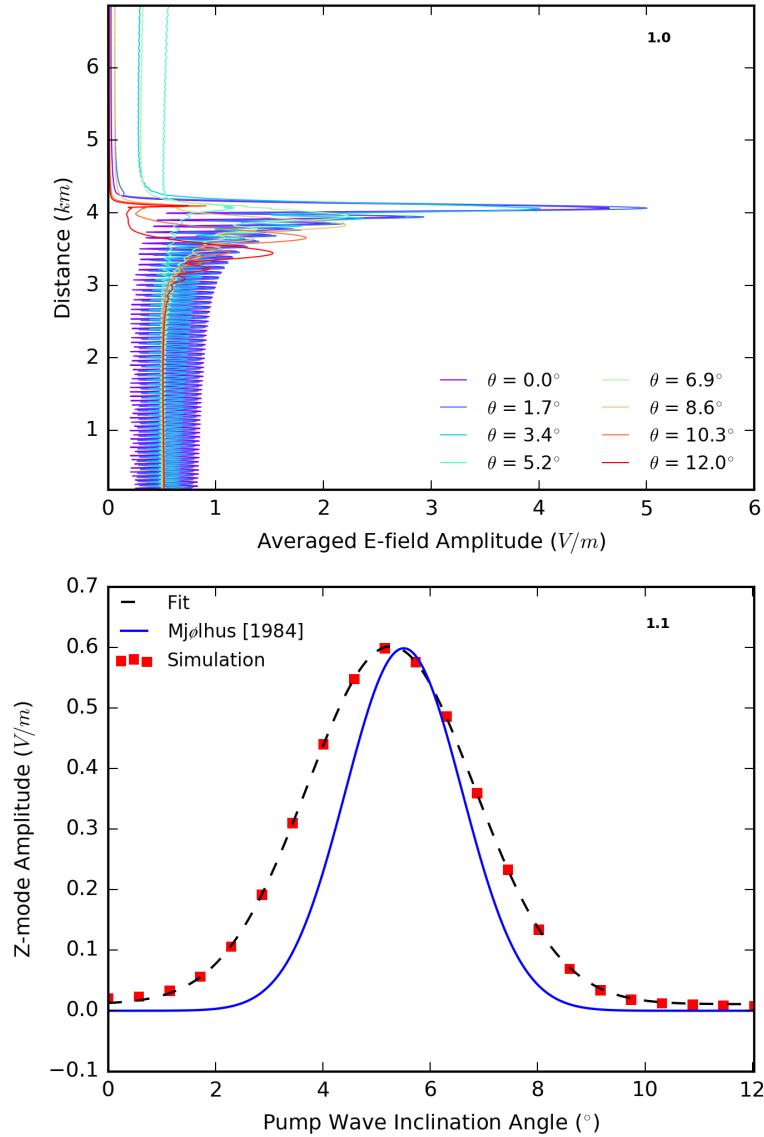


Figure 1: Angular dependence of O-mode to Z-mode conversion for linear vertical density gradient. Upper panel (1.0) shows E-field amplitude averaged over 9.17×10^{-4} s (1×10^5 time steps) for a selection of inclination angles. Penetration of the O-mode reflection height 4.1km above the lower plane of the computational domain can be seen to occur most effectively for angles close to the Spitze at 5.5° . Lower panel (1.1) shows the simulated radio transmission window (red points, dashed black Gaussian fit) and the theoretical prediction from [Mjølhus, 1984] (blue).

time for a steady E-field pattern to develop, but short compared to the timescales required for electron plasma density and temperature perturbations due to the action of the radio wave to develop.

Each trace in the upper panel (panel 1.0) of Figure 1 shows the time averaged E-field amplitude measured along the original direction of propagation for a selection of simulated launch angles. In each case, a swelling effect can be seen as the pump wave approaches the $X^{num} = 1$ point at z_c where the wave is reflected (X^{num} is a numerical equivalent of variable X which takes into account the dispersive and dissipative effects of the discrete computational grid [Cummer, 1997]). At this point the O-mode pump wave is reflected downwards, leading to the generation of the large-amplitude standing waves visible in each plot around the interaction height. In most cases it can be seen that little or no wave amplitude is able to penetrate beyond the O-mode reflection point, however it is apparent that there is a window around 6° for which propagation to higher altitudes is viable. This window is the range of angles for which mode conversion from the initial ordinary wave to an extraordinary-polarized Z-mode wave is favourable, and corresponds to a set of angles for which the \mathbf{k} vector of the incident wave is close to parallel to the local geomagnetic field as the wave reaches the reflection height. The optimal angle for this process to occur in a vertically-inhomogeneous ionosphere is given by the Spitze angle (8) and is a function of the plasma medium parameters, where $Y = \frac{\omega_{ce}}{\omega_0}$, ω_{ce} is the electron cyclotron frequency and α is the angle between

the local geomagnetic field and the vertical.

$$\theta_{Spitze} = \arcsin \left[\left(\frac{Y}{Y+1} \right)^{\frac{1}{2}} \sin(\alpha) \right] \quad (8)$$

In the scenario described here, the value of the Spitze angle was calculated to be 5.5° . The theoretical propagation paths for rays of varying inclination angle in the ionosphere can be seen, for example, in Figure 1 of [Isham *et al.*, 2005]. The average fraction of wave amplitude penetrating beyond the O-mode reflection height for each angle is indicated in the lower panel (1.1) of Figure 1 by the red markers, and shows a Gaussian-shaped transmission window centred on 5.3° and with a full-width at half-maximum of 3.1° (Gaussian fit is indicated by the dashed black line). The theoretical window for transmission of the EM wave through the reflection barrier via O-to-Z conversion as calculated by Mjølhus [Mjølhus, 1984] for the density profile used here is indicated by the blue line.

A small E-field swelling at the reflection height is seen in the upper panel of Figure 1 for waves directed close to the Spitze angle despite the Z-mode conversion efficiency being close to 100%. This is due to a combination of effects: anisotropic divergence in wave direction due to numerical dispersion and the slight spread in propagation angle around the pump wave edges both lead to the reflection of a small fraction of the pump wave.

The linear density slope used in the simulation is only a simplified representation of the F-region of the ionosphere. Experiments such as [Kosch *et al.*, 2011] have observed the magnetic zenith effect to manifest most strongly for inclination angles between the Spitze and field-aligned directions. [Isham *et al.*, 2005] have observed the maximum topside backscattered power to occur in this range, indicative of the radio window shifting towards the magnetic zenith. One mechanism that may be responsible for this shift is the presence of a horizontal density gradient in addition to the vertical gradient. As mentioned in Section 1 above, a varied hierarchy of density structures are likely to arise when the ionosphere is illuminated by high-power radiation due to the formation of plasma irregularities of different scales. In particular, the density gradient in the horizontal direction is unlikely to be homogeneous as assumed in the above analysis. [Honary *et al.*, 2011] obtained a theoretical expression for the shift in the radio window from the Spitze angle towards the magnetic zenith, however this calculation assumed that the ionospheric inhomogeneity existed along one direction only (which in the general case can deviate from the vertical direction). The case of 2D variation on the plasma density has not been discussed before, and can only be investigated numerically.

To this end, the FDTD code was used to investigate the effect that density structures of various spatial scales have on the position of the Z-mode window. Three different inhomogeneity regimes were investigated: large-scale 2D linear gradients, single field-aligned duct-like density depletions and periodically-arranged smaller-scale field aligned irregularities.

To simulate a large-scale density-depleted patch, such as that caused by the bunching together of several non-linear density structures in the heated volume, a linear horizontal slope of scale size L_x with density increasing from left to right in the computational domain was added to the background electron density profile. Examples of the 2D background electron density profiles for a selection of L_x can be seen in the upper panels of Figure 2 (panels 2.0a-g). A computational domain of dimensions $1920 \times 1 \times 1920$ was used, with the discrete step sizes set to $\Delta_t = 4.58 \times 10^{-9} s$ and $\Delta_x = 2.75 m$. All other simulation parameters were set as described above. The full form of the background density profile in this case is given by (9).

$$N_0(x, z) = N_{crit} \left(1 + \frac{x}{L_x} \right) \left(1 + \frac{z - z_{crit}}{L_z} \right) \quad (9)$$

The vertical slope scale size was kept constant at $L_z = 20 km$. The position and width of the Z-mode window was measured for different grades of horizontal slope, changed by varying L_x , with the results shown in Figure 2. The introduction of a horizontal density inhomogeneity of this form was found to shift the centre of the radio window away from the Spitze direction and towards the magnetic zenith direction, with larger shifts experienced as the gradient was increased. The angular width of the window was also found to increase overall as the horizontal gradient increased, whereas the maximum transmitted E-field amplitude was found to decrease. This result supports the theory that the observed angular position of peak magnetic zenith effect could be explained by the presence of a horizontal density slope. For the vertical plasma gradient used here, a peak in the Z-mode window at around $\theta \simeq (8 - 10)^\circ$ would correspond to a horizontal inhomogeneity of around $L_x \simeq 50 km$. In the auroral ionosphere, horizontal gradients in the opposing direction (increasing from right to left in the simulation domain) may also exist. In this case, the density gradient has the effect of shifting the centre of the Z-mode window away from the Spitze and towards the vertical direction, again with a greater deviation occurring for a greater steepness of horizontal slope.

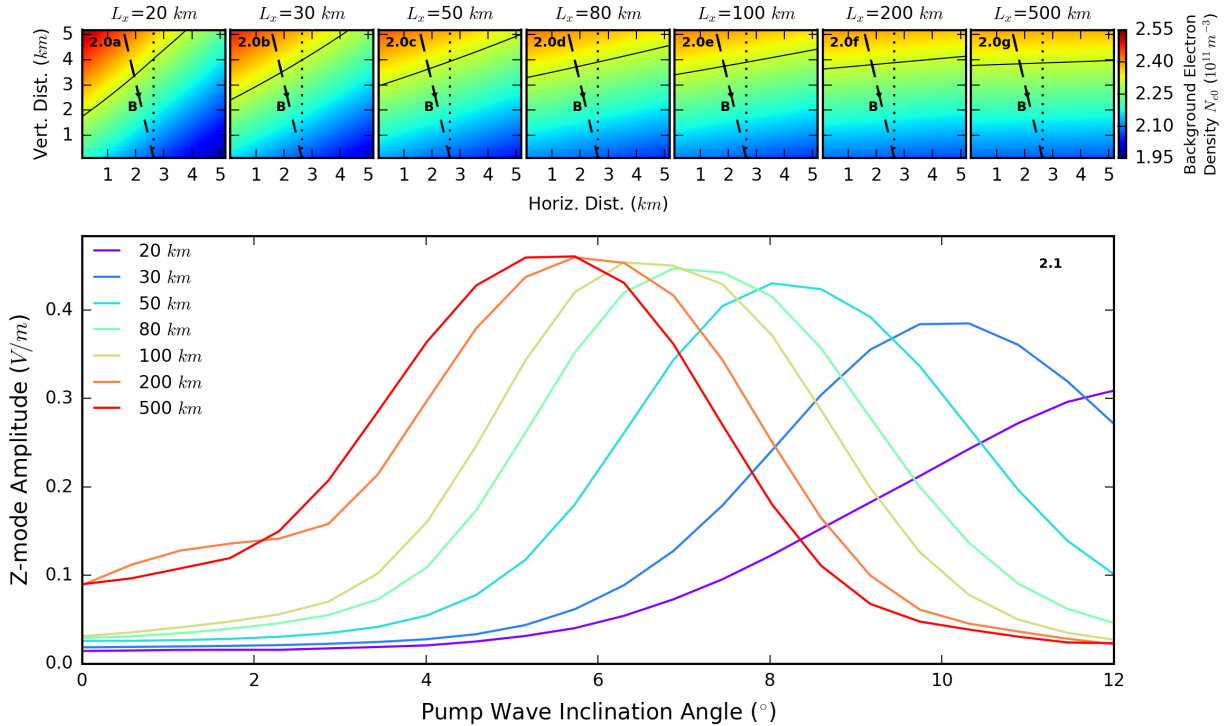


Figure 2: Simulated Z-mode window for varying horizontal slope scale size L_x when background density profile (9) is used as a background density profile (smaller L_x implies a steeper slope). It can be seen that increasing the steepness of the slope shifts the centre of the radio window away from the Spitzze direction and towards the magnetic zenith. The background plasma density, magnetic field direction (dashed line), vertical direction (dotted line) and position of the O-mode reflection height (solid black line) used for each L_x are shown in upper panels 2.0a-g.

To simulate the effects of a duct-like horizontal density feature, a field-aligned density depletion of the form (10) was included in the background density profile.

$$N_{irreg}(x', z') = N_0(x', z') \left[1 - A_{irreg} \exp\left(-\frac{(x_0 - x')^2}{2L_{width}^2}\right) \right] \quad (10)$$

where x' and z' are coordinates perpendicular and parallel to the simulated geomagnetic field, A_{irreg} and L_{width} are the amplitude and width of the irregularity respectively, x_0 is a reference distance, and $N_0(x', z')$ is the vertically-inhomogeneous background density profile given by (7), with the vertical slope scale height kept at $L_z = 20 \text{ km}$ as before. A_{irreg} was set to be 0.05 to represent a maximum density depletion of 5% of the background. A smaller computational domain of dimensions $1280 \times 1 \times 1280$ was used to reduce computing time, with the discrete step sizes set to $\Delta_t = 9.17 \times 10^{-9} \text{ s}$ and $\Delta_x = 5.50 \text{ m}$. L_{width} was varied to investigate a range of irregularity scale-sizes, from small-scale single striations with a width of tens of metres, up to larger ducts with widths of several km . Examples of the 2D background electron density profiles for a selection of L_{width} can be seen in the upper panels of Figure 3 (panels 3.0a-g). The effect of different perturbation widths on the position of the radio window is shown by Figure 3.

The presence of the irregularity was found to have a strong effect on the O- to Z-mode conversion process, with the resulting radio window falling into one of several broad regimes depending on the irregularity width. Smaller-scale irregularities with widths $\lesssim 0.1 \text{ km}$ were found to have a minimal effect on the Z-mode window shape, resulting in only a slight shift the radio window away from the Spitzze position and towards vertical by $(0.5 - 1)^\circ$ measured. For duct widths in this range, the radio window was found to be broader than in the unperturbed case, with a full-width at half-maximum in the range $(4.0 - 4.5)^\circ$. Increasing the perturbation width in the range $0.1 \text{ km} \lesssim L_{width} \lesssim 2 \text{ km}$ was found to lead to an abrupt change in radio window shape, with a significant fraction of incident wave amplitude transmitted as a Z-mode for all sampled angles. This manifested as a broadening of the window as the scale size of the irregularity was increased, with the angular width of the window for a duct of 1 km width almost three times that of the 1D slope case. Increasing the irregularity width also had the effect of decreasing the Z-mode amplitude at each sampled angle, leading to a flattening of the window. For a 1 km width irregularity, the average amplitude transmitted of the Z-mode less than half that transmitted at the

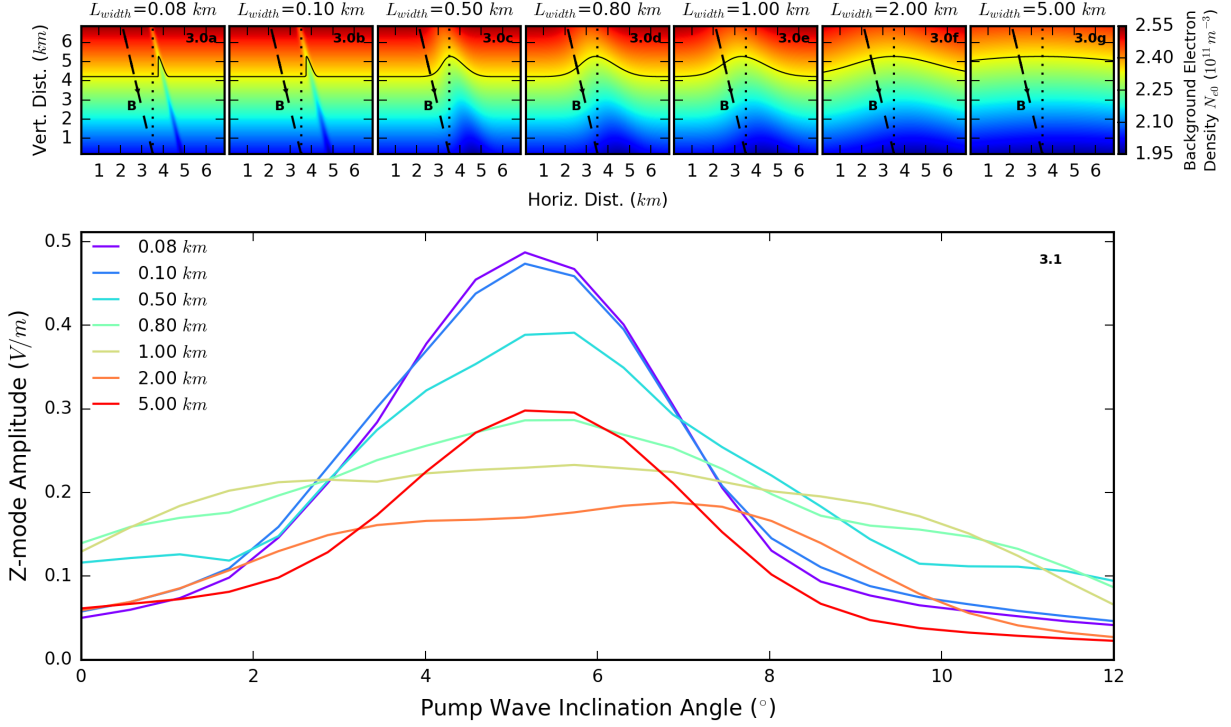


Figure 3: Simulated Z-mode window for varying duct width L_{width} when density perturbation of (10) is included in the background density profile. Initial amplitude of perturbation was set as 5% of the unperturbed background density given by (7). Smaller-width structures with $L_{width} \leq 0.1\text{km}$ can be seen to shift the distribution away from the Spitzze direction towards vertical by $(0.5 - 1)^\circ$. As the irregularity width increases, the window broadens and loses its Gaussian shape. For widths $\geq 0.2\text{km}$, a significant fraction of incident wave amplitude was transmitted at all sampled angles, leading to a dramatic widening and flattening of the window. The background plasma density, magnetic field direction (dashed line), vertical direction (dotted line) and position of the O-mode reflection height (solid black line) used for each L_{width} are shown in upper panels 3.0a-g.

window central angle for the 1D slope regime. As the irregularity width was increased beyond 2 km , the shape of the Z-mode window was found to tend towards the unperturbed form measured for the case of a linear vertical slope only.

Figure 4 shows the E-field amplitude developed in the simulation domain and averaged over $9.17 \times 10^{-4}\text{ s}$ (1×10^5 time steps) for pump wave inclination angles of 0.6° , 2.9° , 5.2° , 7.4° , 9.7° and 12.0° and for the cases of irregularities of width 0.08 , 0.10 , 0.20 , 0.50 and 0.80 km . The colour range of this plot has been logarithmically-normalised to more clearly show the transmitted Z-mode waves. The position of the $X=1$ O-mode reflection contour is marked by a solid line. The Z-mode can be identified as signal which is able to penetrate beyond the O-mode reflection height. Around the region of the duct it can be seen that the Z-mode is transmitted as one or more narrow beams only, with the point(s) of transmission varying greatly according to the pump wave angle and duct geometry. For irregularities of width $> 0.1\text{ km}$, it can be seen that a strong Z-mode beam is transmitted for all angles shown (albeit emerging from very different points of the duct), leading to the flat, broad window profiles shown in Figure 3. Away from the region around the duct, behaviour reverts to that of the unperturbed case described above, with optimal O- to Z-mode conversion occurring at the Spitzze angle. Only waves transmitted within a full width of the irregularity central axis were considered when calculating the shape of the window.

The effect of including multiple periodically-arranged field-aligned density depletions was investigated by including density irregularities of the form (11) to the background density profile.

$$N_{irreg}(x', z') = N_0(x', z') \left\{ 1 - \frac{1}{2} A_{irreg} \left[1 - \cos \left(\frac{2\pi x'}{L_{width}} \right) \right] \right\} \quad (11)$$

Similarly to the duct-like irregularity simulation above, computational domain dimensions of $1280 \times 1 \times 1280$ were used, with the discrete step parameters set to $\Delta_t = 9.17 \times 10^{-9}\text{ s}$ and $\Delta_x = 5.50\text{ m}$. The vertical slope scale size was set to be $L_z = 20\text{ km}$ as before. Figure 5 shows the E-field amplitude developed in the simulation domain and averaged over $9.17 \times 10^{-4}\text{ s}$ (1×10^5 time steps) for pump wave inclination angles of 0.6° , 2.9° , 5.2° ,

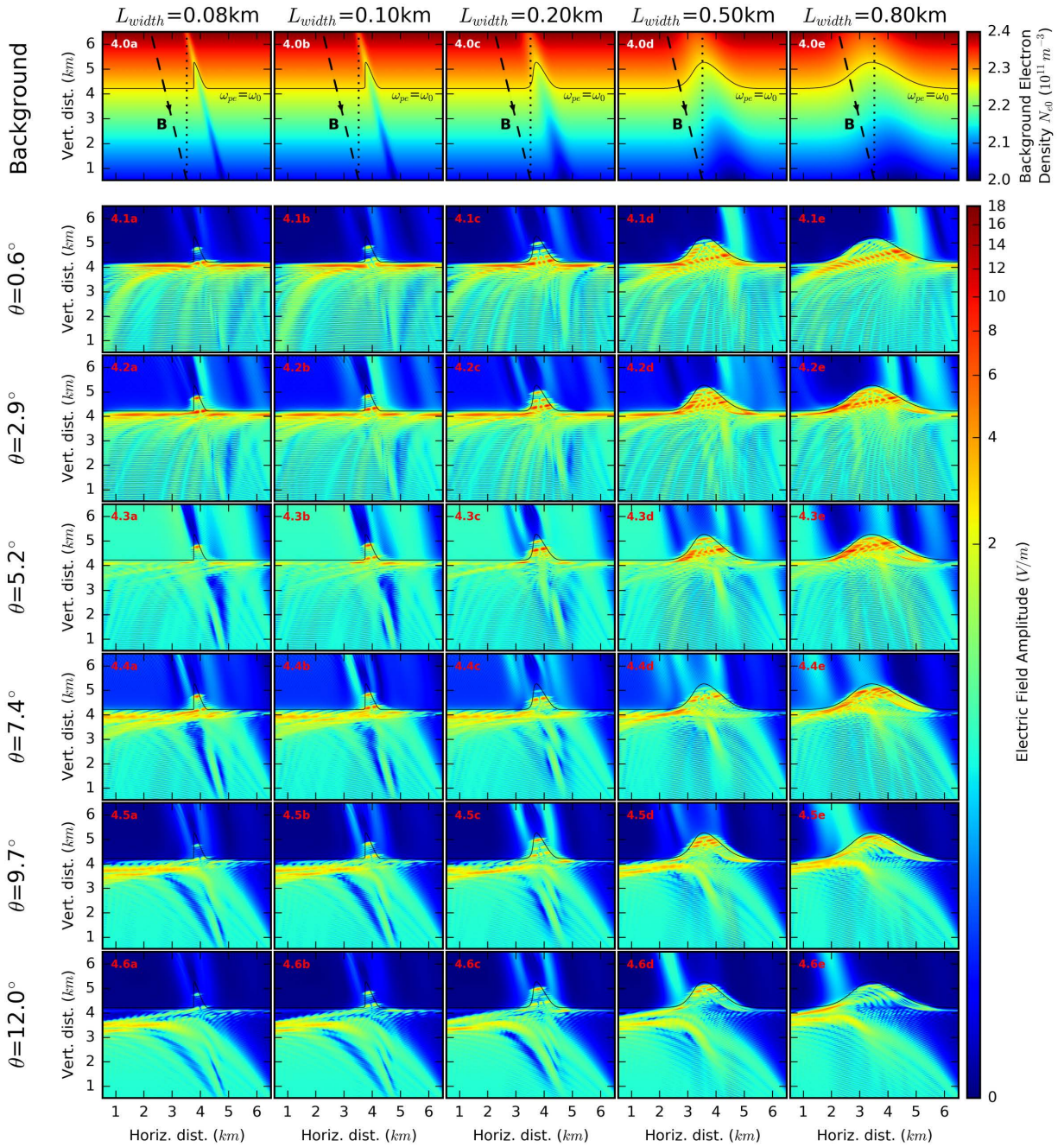


Figure 4: Time-averaged E-field amplitude for pump wave inclination angles of 0.6° , 2.9° , 5.2° , 7.4° , 9.7° and 12.0° when density perturbations of the form (10) and with L_{width} s of 0.08, 0.10, 0.20, 0.50 and 0.80 km are included in the background density profile. The position of the $X = 1$ O-mode reflection contour marked by a solid line. The colour range has been logarithmically-normalised to more clearly show the transmitted Z-mode waves passing beyond the O-mode reflection height. Upper panels (4.0a-e) show the background electron density, position of the O-mode reflection layer (solid black line), vertical direction (dotted black line) and magnetic field direction (dashed black line) for each L_{width} condition.

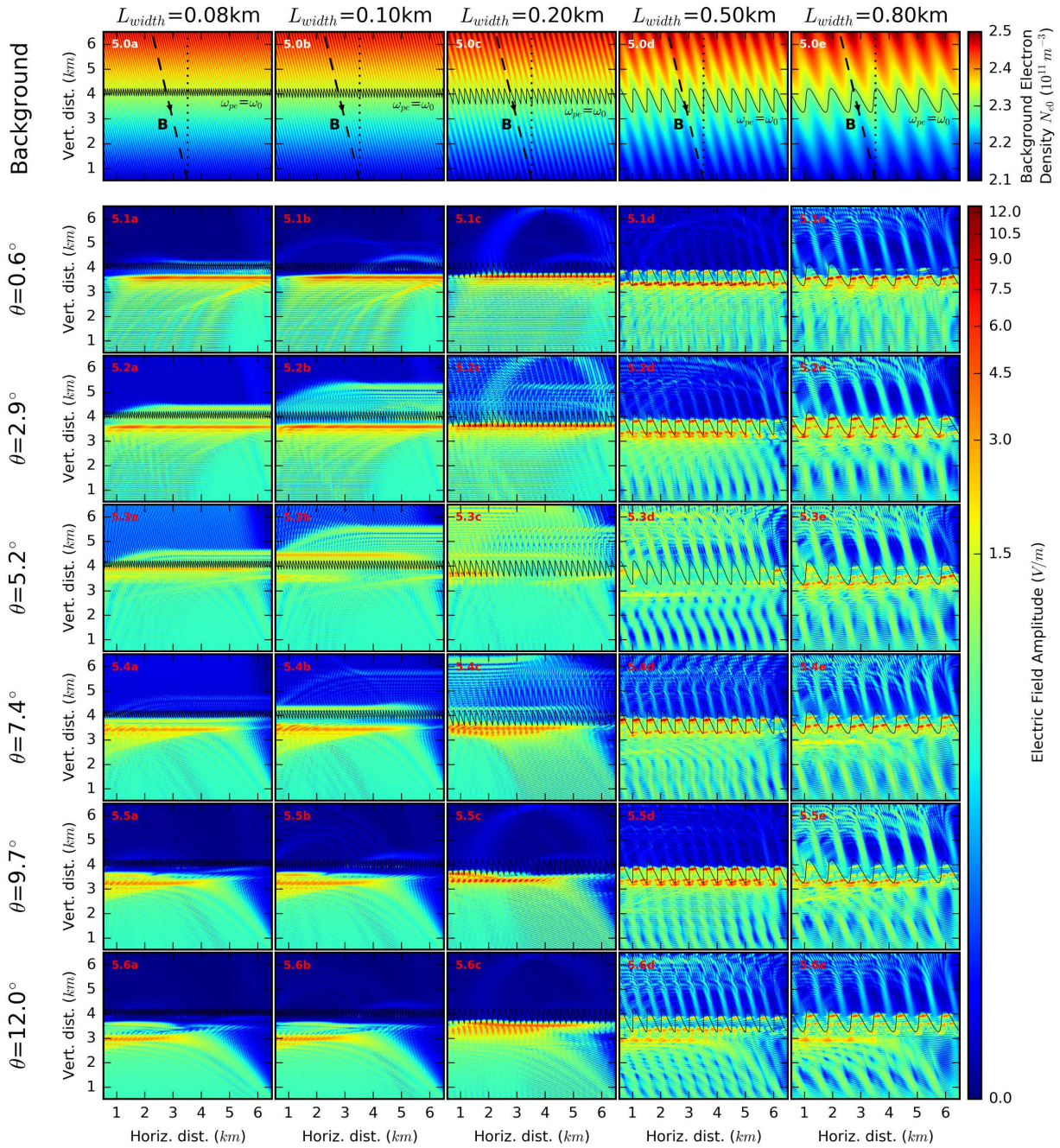


Figure 5: Time-averaged E-field amplitude for pump wave inclination angles of 0.6° , 2.9° , 5.2° , 7.4° , 9.7° and 12.0° when periodic density perturbations of the form (11) and with L_{width} s of 0.08, 0.10, 0.20, 0.50 and 0.80 km are included in the background density profile. The position of the $X = 1$ O-mode reflection contour is marked by a solid line. The colour range has been logarithmically-normalised to more clearly show the transmitted and scattered Z-mode waves beyond the O-mode reflection height. Upper panels (5.0a-e) show the background electron density, position of the O-mode reflection layer (solid black line), vertical direction (dotted black line) and magnetic field direction (dashed black line) for each L_{width} condition.

7.4°, 9.7° and 12.0° and for the cases of periodic irregularities of $L_{width} = 0.08, 0.10, 0.20, 0.50$ and $0.80 km$. As with the single-irregularity case above, the $X = 1$ contour is shown by a solid line and the colour bar has been logarithmically-normalised to more clearly show any transmitted or trapped waves. The 2D background electron density profiles for each L_{width} can be seen in the upper panels of Figure 5 (panels 5.0a-e). In the case of a single duct the transmitted Z-mode wave can emerge from either side of the structure, or even multiple points simultaneously, depending on the inclination angle of the source wave, as shown by Figure 4. In the case of periodic structures, this results in a converted Z-mode potentially entering multiple adjacent irregularities before emerging. This has a strong effect on the propagation of the converted Z-mode, with transmitted waves multiply scattered by adjacent irregularities making it difficult to measure the Z-mode window shape. In general the scattering effect of periodic irregularities with spatial scales comparable to or smaller than the pump wave wavelength ($\leq 0.08 km$) had the effect of attenuating the transmitted Z-mode amplitude at all angles while maintaining the angular window shape measured for the unperturbed case. As the irregularity width increased, multiple scattering of the Z-mode wave between adjacent irregularities resulted in the presence of high-amplitude E-field waves beyond the O-mode reflection height for all sampled pump wave angles. Scattered field beyond the reflection height was found to have amplitudes comparable to that found in the Airy field below the reflection height, and in some cases was well in excess of the maximum Z-mode amplitude obtained beyond $X = 1$ for the unperturbed 1D slope case (shown in Figure 1).

4. Numerical Simulation of Heating Effects

In the previous Section, the FDTD code was used to show that the O-to-Z-mode conversion process is strongly dependent on the electron plasma profile around the interaction height. In this Section, simulation results demonstrating that such behaviour can directly lead to an angular dependence in heating-induced effects such as electron temperature enhancement and the growth of density-depleted field-aligned irregularities are presented.

In an idealized heating experiment with a 1D linear vertical electron density gradient only, an O-mode wave launched at the Spitz angle will be almost fully converted to the Z-mode as it approaches the interaction height. The converted Z wave passes beyond the O-mode reflection barrier and, provided the ionospheric peak density is sufficiently high, is reflected at $X = Y + 1$. The reflected Z-mode wave can then freely propagate downwards, back towards the interaction region. As it approaches the point where $X = (1 - Y^2)/(1 - Y^2 \cos^2 \alpha)$, close to the O-mode reflection height, the reflected Z-mode wave encounters the X-mode resonance layer. This resonance is normally inaccessible to ground-launched fast X-mode waves which are reflected at $X = 1 - Y$, but when excited results in the very efficient conversion of the EM wave to upper hybrid plasma waves [Gondarenko *et al.*, 2002]. This process leads to a large increase in the E-field amplitude around the interaction region as shown in Figure 6. In this Figure, the time-averaged E-field amplitude measured along the direction of propagation is shown for a selection of inclination angles (panels 6.0-6.4). The simulation parameters described in Section 3 for the case of an undisturbed 1D vertical density gradient were used, along with simple linear background electron and ion density profiles as given by (7), with $L_z = 20 km$. The blue curve shows E-field amplitude for the case when a perfectly-matched layer (PML) was used to absorb the Z-mode wave as it reaches the upper boundary of the simulation, suppressing its reflection. The dashed-red curve shows the same signal, but for the case that the upper boundary of the simulation was set to be a reflecting boundary to simulate the reflection of the Z-mode wave at higher altitudes. A partial reflector was used in preference to a perfect reflector as the Z-mode wave would expect to experience partial attenuation due to collisional damping, particularly as it approaches $X = Y + 1$. The variation in the peak E-field amplitude in the interaction region with pump wave inclination angle between the Z-mode-reflection-allowed and Z-mode-reflection-suppressed cases is shown in the lower panel (6.5) of Figure 6. Allowing the Z-mode wave to reflect and propagate back towards the resonance layer was found to lead to a significantly enhanced amplification of the E-field around the interaction region. This effect was particularly pronounced for waves directed towards the centre of the radio window at around 5.5° from vertical, with the maximum magnitude of E-field amplitude found to be greater than 6 times that developed under similar conditions with Z-mode reflection suppressed.

The ability of the reflected Z-mode to excite large-amplitude plasma waves makes a clear difference to the magnitude of E-field standing wave that forms around the interaction region and can drive the formation of artificially-induced perturbations to the plasma medium. To investigate the impact of this on the growth of temperature and density perturbations in the heated region, two parallel simulations were performed: the first with Z-mode reflection suppressed using a PML layer at the upper boundary of the computational domain, the second with Z-mode reflection allowed through the inclusion of a reflecting boundary as described above. The simulation domain was set up with the smaller dimensions of $896 \times 1 \times 640$ Yee cells. The smaller size reduced the computing time required to calculate each simulation cycle and allowed longer-duration runs to be performed. The time step size was set to be $1.83 \times 10^{-8} s$. The Courant number was maintained at 0.5 to preserve stability, and

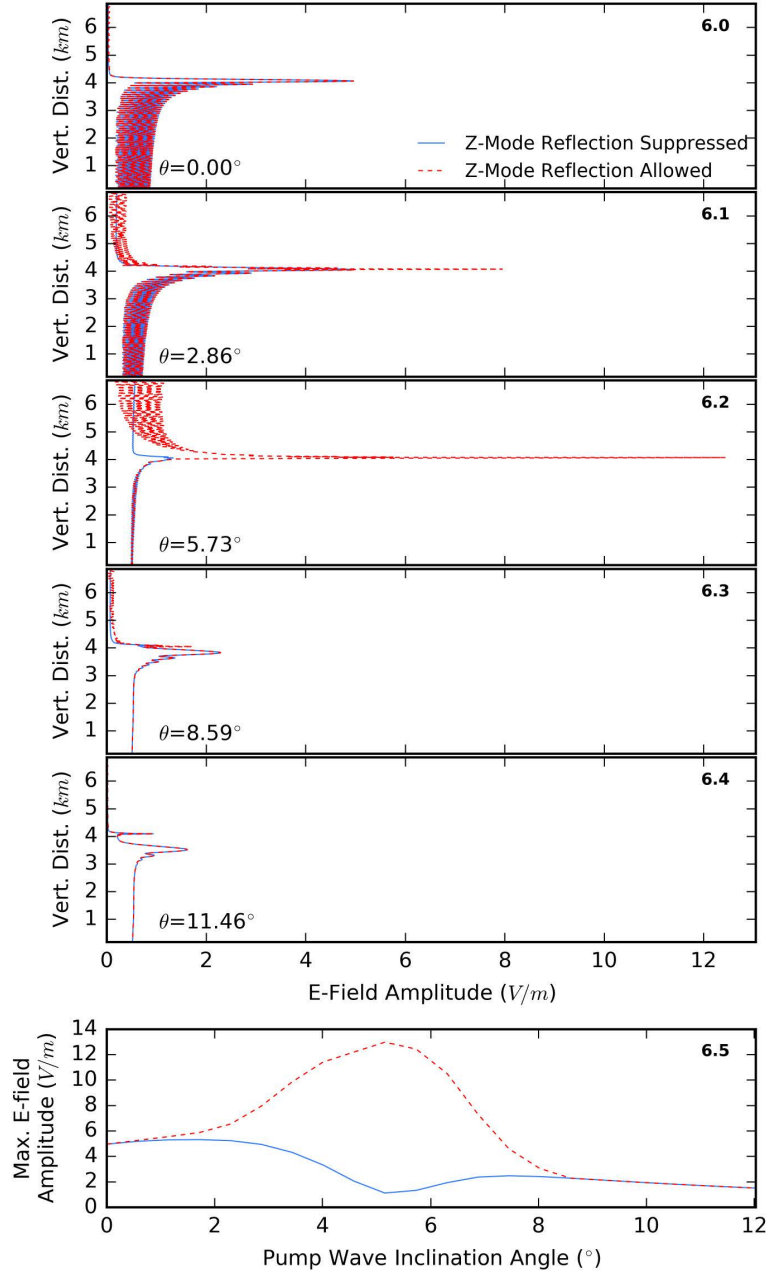


Figure 6: Panels 6.0-6.4 show comparison of the E-field amplitude averaged over 1×10^5 time steps (9.17×10^{-4} s) for the case that the upwards boundary of the computational domain is terminated with an absorbing PML (blue) or a reflecting layer (red-dashed). Traces are shown for a selection of initial pump wave inclination angles. Panel 6.5 shows the variation of maximum averaged E-field amplitude with inclination angle. It can be seen that allowing the Z-mode wave to reflect enhances the amplification of E-field around the interaction region, particularly for waves directed towards the centre of the radio window around 5.5° .

the discrete spatial step size set to be 11.0 m in all directions. A vertical gradient (7) was used as the background density profile with $L_z = 20\text{ km}$, and $z_c = 4.46\text{ km}$ above the bottom edge of the simulation box, as indicated the 2D background density plots shown in Figure 7 (panel 7.0) and Figure 8 (panel 8.0). Initially, no horizontal inhomogeneity was included. For this background density profile, the upper-hybrid resonance point occurred at 3.16 km above the bottom edge of the simulation. This domain set-up was designed to include the important regions of interaction such as the reflection and upper hybrid resonance heights, while keeping the overall domain size small to reduce the computational run-time. An O-mode pump wave of frequency $\omega_0 = 2\pi \times 4.54\text{ MHz}$ was launched at an angle of 5.16° from the lower edge of the computational domain. As this inclination angle is close to the centre of the radio window, it was expected to lead to efficient conversion of the pump wave to the Z-mode.

The beam was given a Gaussian profile to keep most of the source wave energy away from the domain boundaries. All other domain parameters were set as described in Section 3 for the case of the undisturbed 1D vertical density gradient.

Figures 7 and 8 illustrate the variation of E-field, electron density perturbation (expressed as a fraction of the background electron density, N_{e0}), fractional electron density irregularity amplitude $\delta N/N_{e0}$, and temperature perturbation evolved in the simulation after 1.83×10^{-4} s, 1.83×10^{-2} s, 9.17×10^{-2} s, 1.83×10^{-1} s, 2.93×10^{-1} s and 1.10 s for the cases of Z-mode reflection suppressed (Figure 7) and allowed (Figure 8). The irregularity amplitude δN is calculated by subtracting a local average (taken along the horizontal x -direction) from the electron density perturbation, such that $\delta N = N_e - \langle N_e \rangle_x$. Both Figures show a rapid rise of the E-field amplitude at around $z_c = 4.46$ km corresponding to the high-amplitude reflected standing wave, which results in significant rise of the E field amplitude and an increase (due to the wave dissipation) of the electron temperature, which saturates after ~ 0.3 s. Allowing the Z-mode to reflect had a significant effect on the E-field strength developed in the simulation, with the saturation E-field amplitude achieved with reflection allowed over 10 times greater than with reflection suppressed. For the case of suppressed reflection, the highest field amplitudes were located around the reflection height at z_c and remained relatively steady for the duration of the simulation. By contrast, with reflection allowed, E-field amplitudes of up to 6 V/m were developed and located in a narrow band initially around z_c corresponding to the location of the resonance. This can be seen to move upwards in altitude with time as the simulation progresses, as shown by panels 8.1-6a of Figure 8. The Z-mode reflection allowed scenario was found to produce around double the increase in temperature compared to the reflection suppressed scenario. For both reflection suppressed and allowed cases, a strong electron density depletion is observed around the region of interaction. In the reflection-suppressed scenario, this takes the form of a pair of density depleted patches located on the shoulders of the Z-mode window. The density depletions are correlated with the regions where the pump wave is reflected and the reflection-induced standing wave forms (towards the edges of the beam, rather than towards the beam centre where the O-mode wave is transmitted as a Z-mode). This suggests that the formation of the density cavities may, in part, be due to a ponderomotive interaction or the excitation of a parametric instability. Around the peak of the window, the EM wave is mostly transmitted as the Z-mode and the swollen-amplitude reflected standing wave does not form; hence the density in this region is comparatively unperturbed. In the reflection-allowed scenario, the density perturbation takes the form of a single density-depleted cavity with a maximum depth of $|N_e^{min}| \sim 0.02N_{e0}$. This is greater by almost a factor of 4 than the maximum magnitude of perturbation observed in the reflection-suppressed simulation. In this case, the site of maximum depletion can be seen to rise in altitude as the simulation progresses. This is caused by the downwards-travelling Z-mode wave encountering a region of plasma that matches the extraordinary-wave resonance condition $X = (1 - Y^2)/(1 - Y^2 \cos^2 \alpha)$ as it enters the depleted density patch. Due to the presence of the depletion, the resonance is encountered at a higher altitude than if there had been no density perturbation. High E-field amplitudes are excited as a result, which accelerates the depletion of density around that region and leads to a gradual rise in altitude of the region of maximum density depletion as the simulation progresses. This process also explains why the band of maximum E-field amplitude moves upwards in altitude with time.

An interesting feature to note is the spontaneous formation of small-scale field-aligned density structures visible at after ~ 0.1 s in the simulation. These are particularly clear in the plots of the density irregularity amplitude shown by Figure 7, panels 7.4c (in which the features are indicated by an arrow) and 7.5c, and can also be seen for the reflection-allowed case in Figure 8, particularly panels 8.4c and 8.5c. These appear to evolve naturally in the simulation, first appearing in a narrow band located just below the point at which the background upper-hybrid frequency matches with the pump wave frequency, and subsequently increase in both depth and elongation with time. At later times they can be seen to bunch together into larger-scale structures. Due to the location and orientation of these structures, it is clear that they are formed in the simulation due to the conversion of the pump wave to upper-hybrid waves; the altitude at which the structures initially form is located just below the upper-hybrid resonance height where the pump wave frequency matches the upper hybrid frequency, and the structures are exactly aligned along the geomagnetic field direction, consistent with a wave propagating in a direction perpendicular to this magnetic field. Changing the position of the upper-hybrid resonance height within the computational domain was found to change the position of this feature, with the initial location of the irregularity perturbation consistently found to originate in a band ~ 400 m below the UHR height before extending with time to both higher and lower altitudes along the magnetic field direction.

Resolvable field-aligned density irregularities were visible after as little as 0.1 s; this was unexpected as similar structures have been observed experimentally to require timescales of a few seconds or more to develop. This discrepancy may be partly due to the low amplitudes of the simulated irregularities: the maximum density irregularity amplitude developed over the simulation run was only $|N_e - \langle N_e \rangle_x| < 0.001N_{e0}$, which may be difficult to detect experimentally in a real heating experiment. The early onset of irregularity development may also be linked to the numerical noise level in the simulation. The linear mode conversion process understood

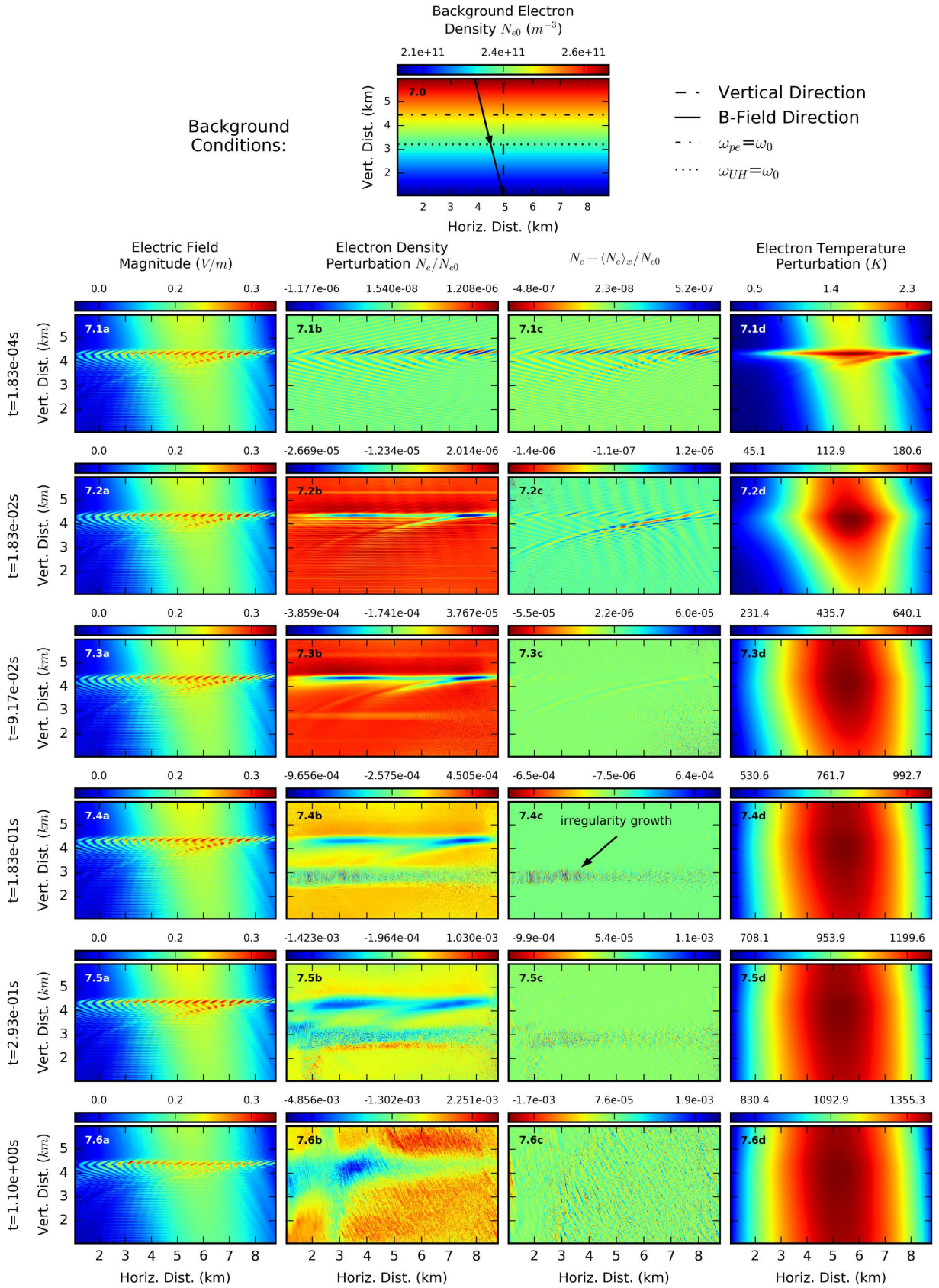


Figure 7: Change in the simulated E-field amplitude, electron density perturbation (expressed as a fraction of the background density N_{e0}), density irregularity amplitude ($N_e - \langle N_e \rangle_x$), and electron temperature perturbation with time, when Z-mode reflection was suppressed. Spatial snapshots of each quantity are shown for times 1.83×10^{-4} s, 1.83×10^{-2} s, 9.17×10^{-2} s, 1.83×10^{-1} s, 2.93×10^{-1} s and 1.10 s. The background density profile, geomagnetic field orientation (solid black line), O-mode reflection height (dot-dashed black line) and upper-hybrid resonance height (dotted black line) are shown in panel 7.0. Field-aligned density irregularities can be seen to grow with time around the UHR height, as indicated in panel 7.4c.

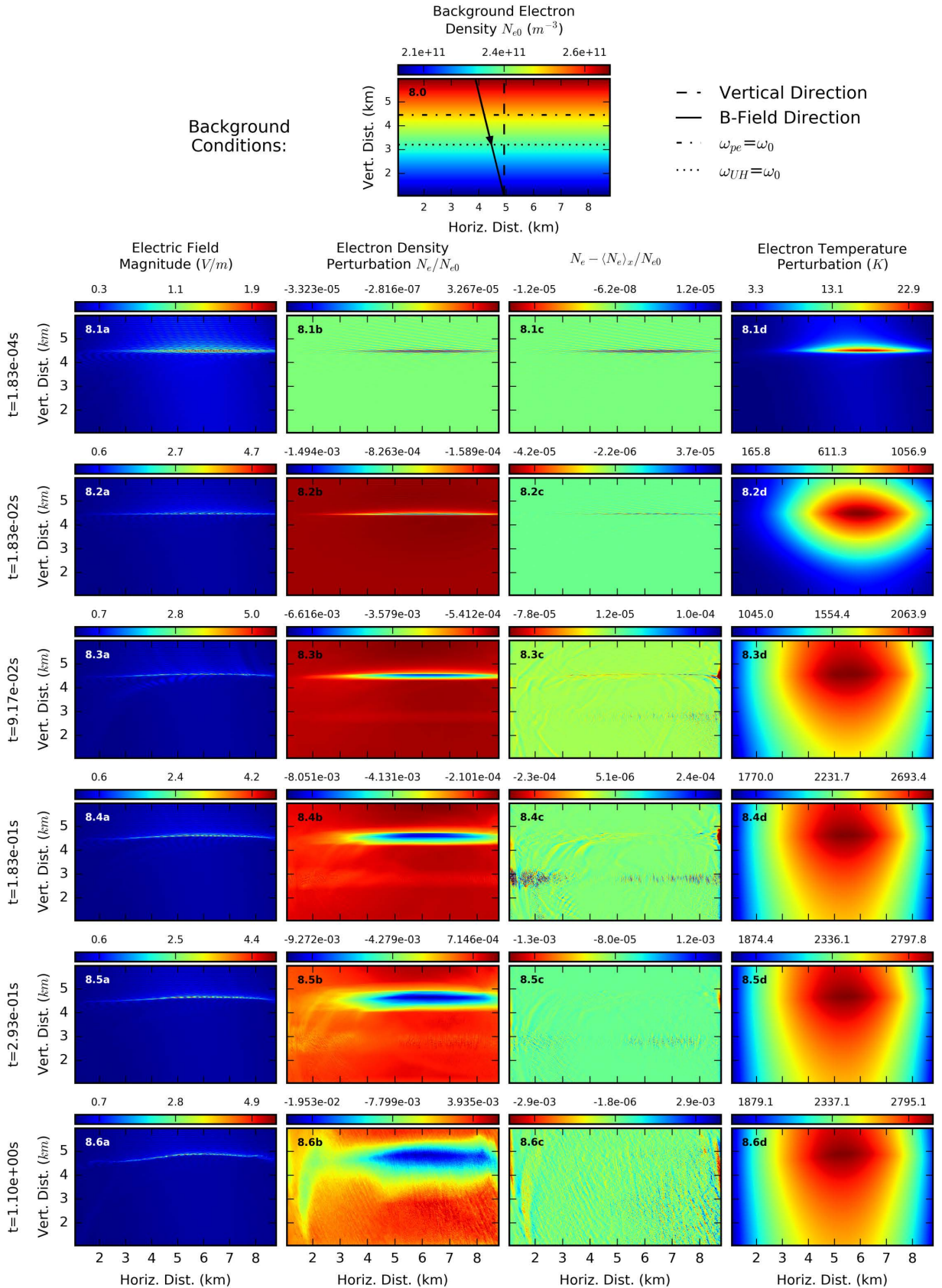


Figure 8: Change in the simulated E-field amplitude, electron density perturbation (expressed as a fraction of the background density N_{e0}), density irregularity amplitude ($N_e - \langle N_e \rangle_x$), and electron temperature perturbation with time, when Z-mode reflection was allowed. Spatial snapshots of each quantity are shown for times 1.83×10^{-4} s, 1.83×10^{-2} s, 9.17×10^{-2} s, 1.83×10^{-1} s, 2.93×10^{-1} s and 1.10 s. The background density profile, geomagnetic field orientation (solid black line), O-mode reflection height (dot-dashed black line) and upper-hybrid resonance height (dotted black line) are shown in panel 8.0.

to govern UH generation from an O-mode pump wave requires small-amplitude seed density irregularities to be present before it may proceed, however no such seed irregularities were included in the initial simulation density profiles. It is likely here that the seed for this process is provided by the low-amplitude numerical noise present in the simulated ion and electron densities. This is an artifact of the computational process and not physical in nature, however it may play an equivalent role to the seeding effect of low-amplitude density variations in the real ionosphere. If the numerical noise is of a higher amplitude or grows at a faster rate than seed perturbations in the real ionosphere, it may explain the unexpectedly early appearance of the field-aligned structures in the simulation.

To investigate this, the simulation was repeated for varying temporal and spatial step sizes, while keeping the Courant number constant. It was found that the field-aligned density structures become visible after approximately $6 \times 10^6 \Delta_t$, regardless of the magnitude of Δ_t , when test simulations were performed for $\Delta_t = 9.17 \times 10^{-9} s$, $\Delta_t = 1.83 \times 10^{-8} s$ and $\Delta_t = 3.67 \times 10^{-8} s$. Subsequent to this, the growth rate of the irregularities was consistent with development due to a thermal physical process such as the resonance instability, and scaled with the simulated time in seconds rather than with the number of time steps. This implies that the onset time of irregularity growth was numerical in nature, dependent on the growth of numerical noise in the simulated plasma density, and thus was determined by the simulation time step number. After the onset of the irregularities, their growth was physical in nature and progressed according to the physical timescale in the simulation rather than the numerical time step.

To investigate the angular dependence of heating induced effects, the simulations were repeated for pump wave launch angles θ of 0.1° , 1.7° , 3.4° , 5.2° , 6.9° and 8.6° . The electron density and temperature perturbation developed after $1.1 s$ for each wave direction is shown in Figure 9, with the Z-mode reflection-allowed case on the left (panels 9.1-6a and 9.1-6c) and Z-mode reflection-suppressed case on the right (panels 9.1-6b and 9.1-6d). In the reflection-allowed scenario, the strongest electron temperature enhancement was found to occur for an angle of 5.2° (shown in panel 9.4c), which supports the argument that the pump wave that converts most efficiently to the Z-mode (in this case, the wave with an inclination angle closest to the Spitze) produces the greatest temperature perturbation. For the reflection-suppressed scenario, the wave launched in a near-vertical direction produced the greatest temperature enhancement (shown in panel 9.1d), as this wave lost the least energy to Z-mode transmission and thus resulted in a greater amplitude of standing wave below the O-mode reflection height. In the reflection-suppressed case, the Spitze-directed wave was almost fully transmitted through the reflection barrier and subsequently absorbed by the PML, hence causing the least temperature perturbation.

Summary plots showing how the maximum value of electron temperature perturbation and the minimum value of electron density perturbation in the simulation domain changed with time can be seen in the lower panels of Figure 9 (panels 9.7a-b), for the cases of the pump wave directed above (8.6°), below (0.0°) and along the Spitze direction (5.2°). The Z-mode reflection-allowed scenario is shown by a solid line, with the reflection-suppressed case indicated by a dashed line. Allowing Z-mode reflection can be seen to lead to a higher eventual magnitude of heating induced effects by as much as a factor of 2 for the case of the Spitze-directed wave. Pump waves with initial inclination angles closer to the Spitze direction (for which conversion to Z-mode was more favourable) were found to achieve a greater magnitude of temperature enhancement and a greater variation between the reflection-allowed and reflection-suppressed cases. The rate of development of temperature enhancement was more rapid in the reflection-allowed case; for example when the incident wave was directed at 5.2° , the steady-state temperature is achieved after $0.25 s$ in the reflection-allowed case, compared with $0.6 s$ in the reflection-suppressed case. This can be attributed to a greater rate of thermal diffusion in the reflection-allowed scenario caused by the much higher temperature, which allowed thermal equilibrium (steady state conditions) to be achieved more quickly.

The pump wave directed close to the Spitze direction was also found to be most effective at exciting small-scale field aligned density irregularities around the upper-hybrid resonance height. This is shown by Figure 10 which displays the change in the fractional electron density irregularity amplitude, $(N_e - \langle N_e \rangle_x) / N_{e0}$, with time in a narrow band of altitude around the UH resonance level. Results are shown for pump waves directed along 0.0° (panels 10.0-4b), 5.2° (10.0-4c) and 8.6° (10.0-4d) to the vertical, after times of $0.11 s$ (uppermost panels; 10.0b-d), $0.13 s$, $0.15 s$, $0.17 s$, and $0.18 s$ (lowermost panels; 10.4b-d). The UH resonance height for which the local UH frequency matches the pump wave frequency ($\omega_{UH} = \omega_0$) is indicated by a dashed line. In each case, clear field-aligned density perturbations can be seen to grow with time, first visible from $\sim 0.1s$ and persisting until they begin to collapse into less-ordered small-scale structures leaving a slight net density depletion. Initial growth of the irregularities in all cases occurs at an altitude $\sim 0.4km$ below the UH height, after which they extend with time to both higher and lower altitudes. The rate of growth of striations can be seen to vary with pump wave angle, with the wave directed closest to the Spitze angle (5.2°) causing the most rapid growth, both in terms of depletion depth and elongation along the magnetic field direction.

Panels 10.0-4a in Figure 10 show the 1D spatial discrete Fourier transform (DFT) of the magnitude of the fractional density irregularity amplitude $\delta N_e / N_{e0} = |N_e - \langle N_e \rangle_x| / N_{e0}$ for each angle, sampled along the hori-

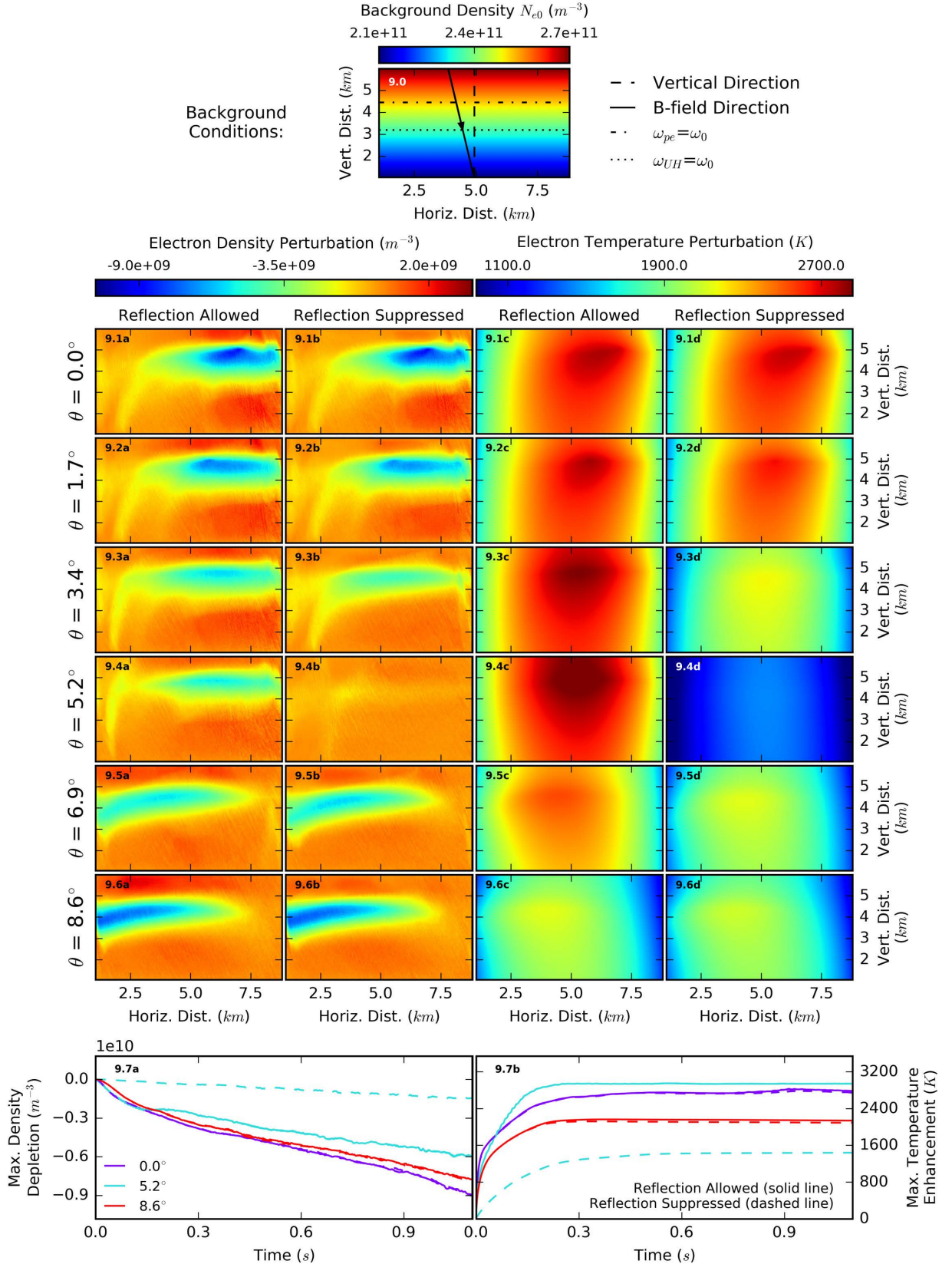


Figure 9: Variation of electron density and electron temperature perturbation with pump wave inclination angle, for the cases that Z-mode reflection is allowed and suppressed. In the reflection-allowed scenario, the strongest electron temperature enhancement was found to occur for an angle of 5.2° (close to the Spitzze angle; shown in panel 9.4c), supporting the argument that the pump wave that converts most efficiently to the Z-mode produces the greatest temperature perturbation. In the reflection-suppressed scenario, the wave launched in a near-vertical direction produced the greatest temperature enhancement (shown in panel 9.1d). The Spitzze-directed wave in the reflection-suppressed case was almost fully transmitted through the reflection barrier and subsequently absorbed by the PML, hence causing the least temperature perturbation (9.4d). The lower panels (9.7a-b) show the variation of the maximum value of electron temperature enhancement and electron density depletion in the simulation domain with time, for the Z-mode reflection allowed (solid lines) and suppressed (dashed lines) scenarios. Background conditions are shown in the upper panel (9.0).

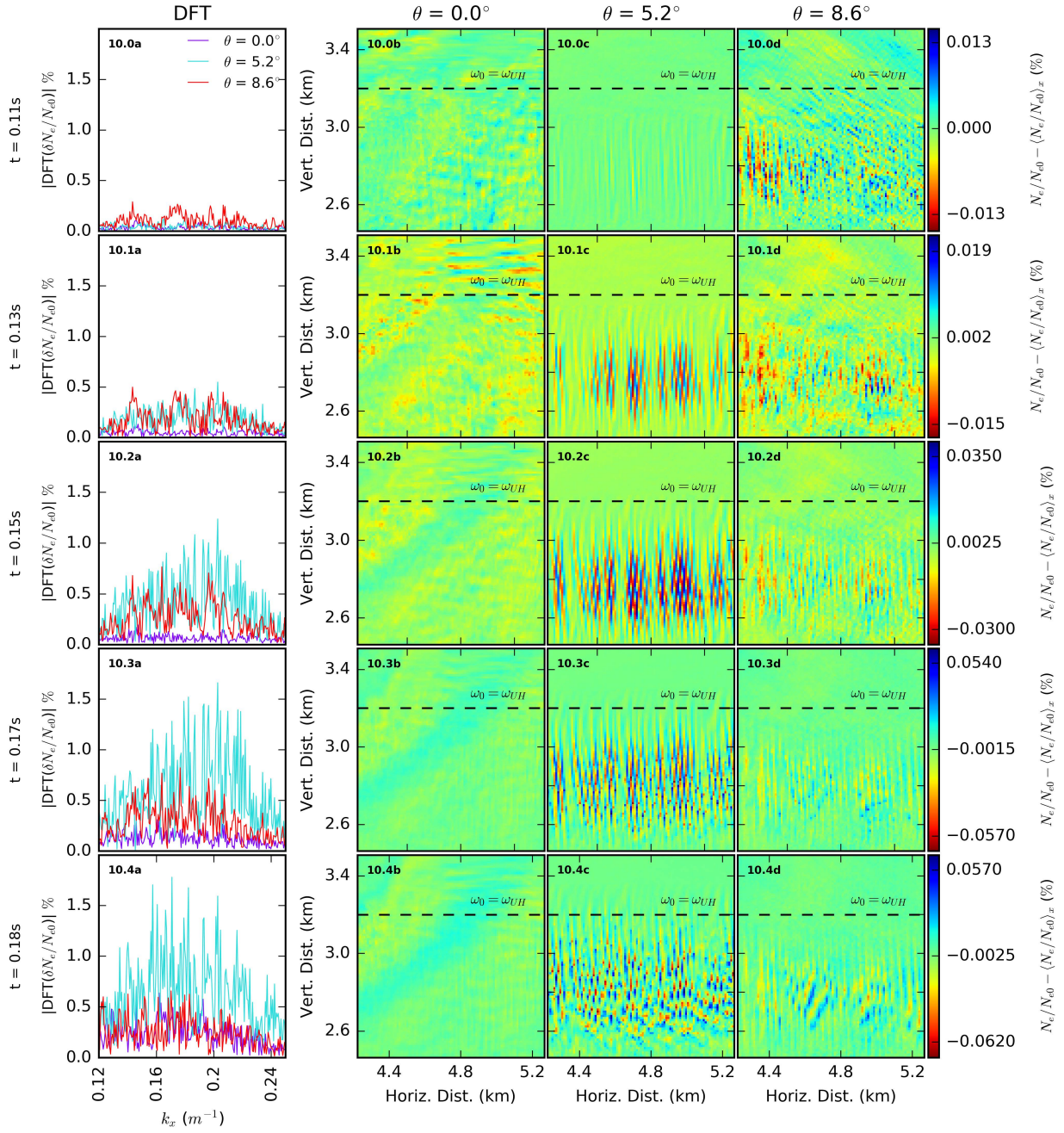


Figure 10: Right-hand columns show the simulated growth of small-scale field-aligned density irregularities with time in a narrow band of altitude below the UH resonance level for pump waves directed along 0.0° (panels 10.0-4b), 5.2° (10.0-4c) and 8.6° (10.0-4d) to the vertical. The UH resonance height is indicated by a dashed line. Left-hand panels (10.0-4a) show the 1D spatial DFT of $\delta N/N_{e0}$ sampled along the horizontal axis of the simulation domain at the height at which the irregularities begin to develop. Amplitude of spatial frequency components around this value increases with time corresponding to the growth of irregularities and is greater by a factor of 2 or more in the case of the 5.2° -directed wave.

zontal axis of the simulation domain at the height at which the irregularities begin to develop. The DFT plots show that there is a clear increase in the perturbation amplitude for spatial frequencies around $k_x \sim 0.18m^{-1}$, which increases in amplitude with time as the irregularities grow. This range of spatial frequencies corresponds to irregularities with scale sizes of 30 – 40 m perpendicular to the geomagnetic field direction. The amplitude of density perturbation components in this scale-size range is highly dependent on pump wave angle, with the amplitude greater by a factor of 2 or more in the case of the Spitze-directed wave. From this it follows that the UH wave excitation process is dependent on wave angle, with UH production occurring most favourably at the same range of angles for which the O- to Z-mode conversion process was most favourable.

Production of UH waves and their dissipation in the associated field-aligned irregularities would be make a significant contribution to the electron temperature enhancement via the resonance instability. As such, the dependence of irregularity production on pump wave angle demonstrated by these simulations could be expected to add a further contribution to the magnetic zenith effect. Small-scale density irregularities such as this may also affect the development of large-scale plasma perturbations through anomalous attenuation of the pump wave. The code used here treats absorption of the pump wave through inclusion of an effective collision term ν_0 in a manner similar to that described by [Gondarenko et al., 2006]. The magnitude of irregularities developed over the simulation timescale is small ($< 0.001N_{e0}$), however, there is a small attenuation in the pump wave amplitude ($< 1 dB$ for the vertically-directed wave) which may be due to absorption caused by irregularities.

These results show that the O-mode to Z-mode conversion process could be an important mechanism behind the observed magnetic zenith effect, with the observed angular dependence arising from the shape of the Z-mode window and the resonant excitation of large-amplitude electric fields via the reflected Z-mode contributing to the enhanced plasma perturbations.

5. Inclusion of Density Structures

The previous Section demonstrates that the O-mode to Z-mode conversion process can lead to a variation in the magnitude of artificial plasma perturbation with the inclination angle of an incident O-mode wave, for the case of a 1D linear vertical plasma density gradient. The addition of a component of horizontal inhomogeneity has been shown in Section 3 to significantly modify the Z-mode window, thus it is to be expected that the presence of a horizontally-inhomogeneous density feature will also affect the dependence of plasma perturbation on pump wave direction. This Section presents the results of simulations performed for various pump wave directions and for the cases that a linear horizontal density gradient, a single field-aligned density-depleted duct, or a periodic distribution of field-aligned density-depleted irregularities are included in the background density profile.

Simulations were performed for pump wave initial inclination angles 0.0° , 2.9° , 5.7° , 8.6° , 11.5° with Z-mode reflection allowed. Computational domain dimensions were set to be $1024 \times 1 \times 768$. For increased accuracy, the time step size was reduced to $1.22 \times 10^{-8}s$, and the spatial step size to 7.33m. All other simulation parameters were set as in Section 4.

The upper panels of Figure 11 show the electron density and temperature perturbation developed in the simulation after 0.23 s when a 2D density profile including a linear horizontal slope as given by (9) was used. Results for horizontal scale size $L_x = 20 km$ (11.1-5a and 11.1-5c) and $L_x = 50 km$ (11.1-5b and 11.1-5d) are shown. In both cases the vertical slope scale-size was set to be $L_z = 20 km$. The lowermost panels show the variation of minimum density perturbation (panel 11.6a) and maximum temperature perturbation (panel 11.6b) recorded in the simulation with time. The $L_x = 20 km$ case is indicated by a solid line, the $L_x = 50 km$ case by a dashed line.

The most striking difference between the results shown in Figure 11 and the unperturbed case with no horizontal inhomogeneity shown in Figure 9 is the shifting of the inclination angle responsible for the greatest temperature enhancement from the Spitze position towards the magnetic zenith direction with decreasing L_x . For $L_x = 50 km$, the greatest temperature enhancement is produced by the wave launched at 8.6° (shown in panel 11.4d). This is consistent with the modification of the Z-mode window found by the simulations reported in Section 3 for the case of a linear horizontal density inhomogeneity, as shown in Figure 2, which predicts maximum Z-mode transmission to occur for pump waves directed at an angle of 8.2° for the $L_x = 50 km$ case. Likewise, the analysis of Section 3 shows O- to Z-mode conversion to be more favourable as the pump wave direction approaches the zenith direction for $L_x = 20 km$, in good agreement with the simulations performed here which show that the temperature enhancement increases as the pump wave inclination angle increases, with maximum enhancement found for the pump wave directed at 11.5° (shown in panel 11.5c).

Similar plots are shown in Figures 12 and 13 for the cases of a single density-depleted field-aligned duct and a periodic distribution of such irregularities respectively. In both scenarios, an inhomogeneities with scale parameters $L_{width} = 0.08 km$ and $L_{width} = 0.8 km$ are compared.

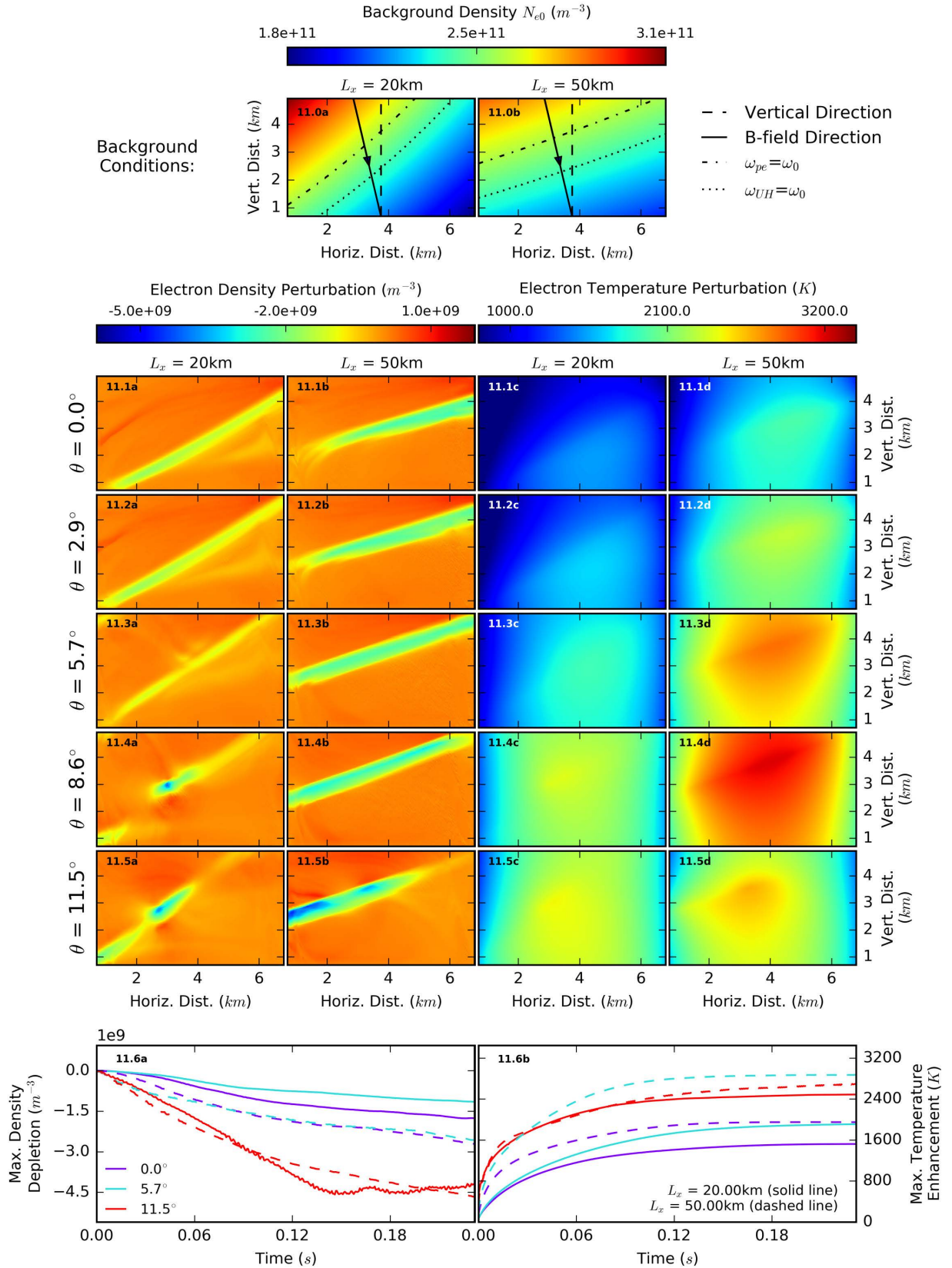


Figure 11: Variation in electron density perturbation and electron temperature perturbation with pump wave inclination angle when horizontal density slopes of the form (9) with $L_x = 20\text{ km}$ and $L_x = 50\text{ km}$ were included in the background density profile. Uppermost panels (11.0a-b) show the background conditions for each L_x case. Lowermost panels (11.6a-b) show the variation of minimum density perturbation and maximum temperature perturbation recorded in the simulation with time for $L_x = 20\text{ km}$ (solid line) and $L_x = 50\text{ km}$ (dashed line). The inclination angle responsible for the greatest temperature enhancement shifts from the Spitzze position towards the magnetic zenith direction with decreasing L_x , consistent with the modification of the Z-mode window simulated in Section 3 (shown in Figure 2).

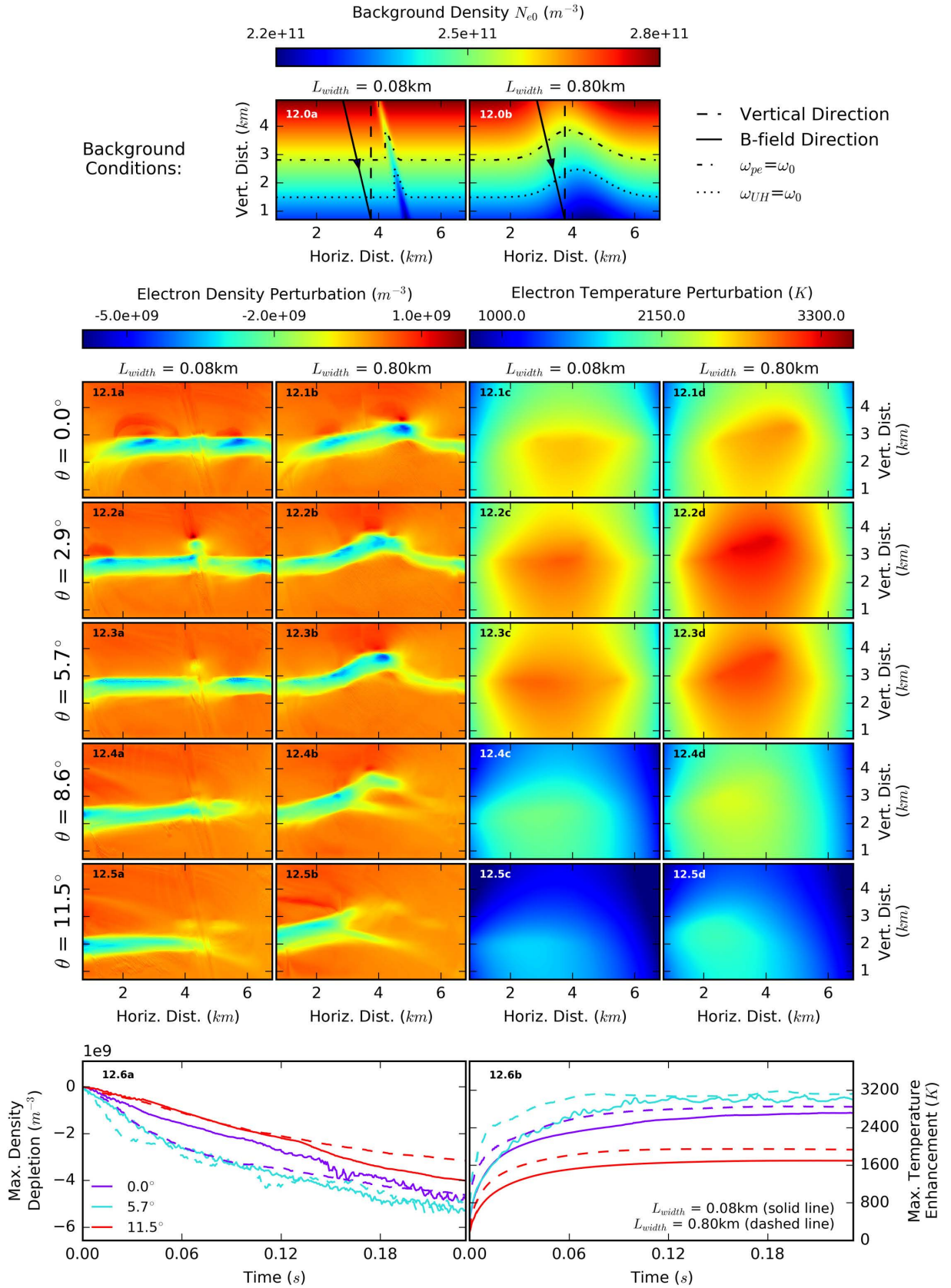


Figure 12: Variation in electron density perturbation and electron temperature perturbation with pump wave inclination angle when single density-depleted field-aligned irregularities of the form (10) with $L_{width} = 0.08 km$ and $L_{width} = 0.8 km$ were included in the background density profile. Uppermost panels (12.0a-b) show the background conditions for each L_{width} case. Lowermost panels (12.6a-b) show the variation of minimum density perturbation and maximum temperature perturbation recorded in the simulation with time for $L_{width} = 0.08 km$ (solid line) and $L_{width} = 0.8 km$ (dashed line).

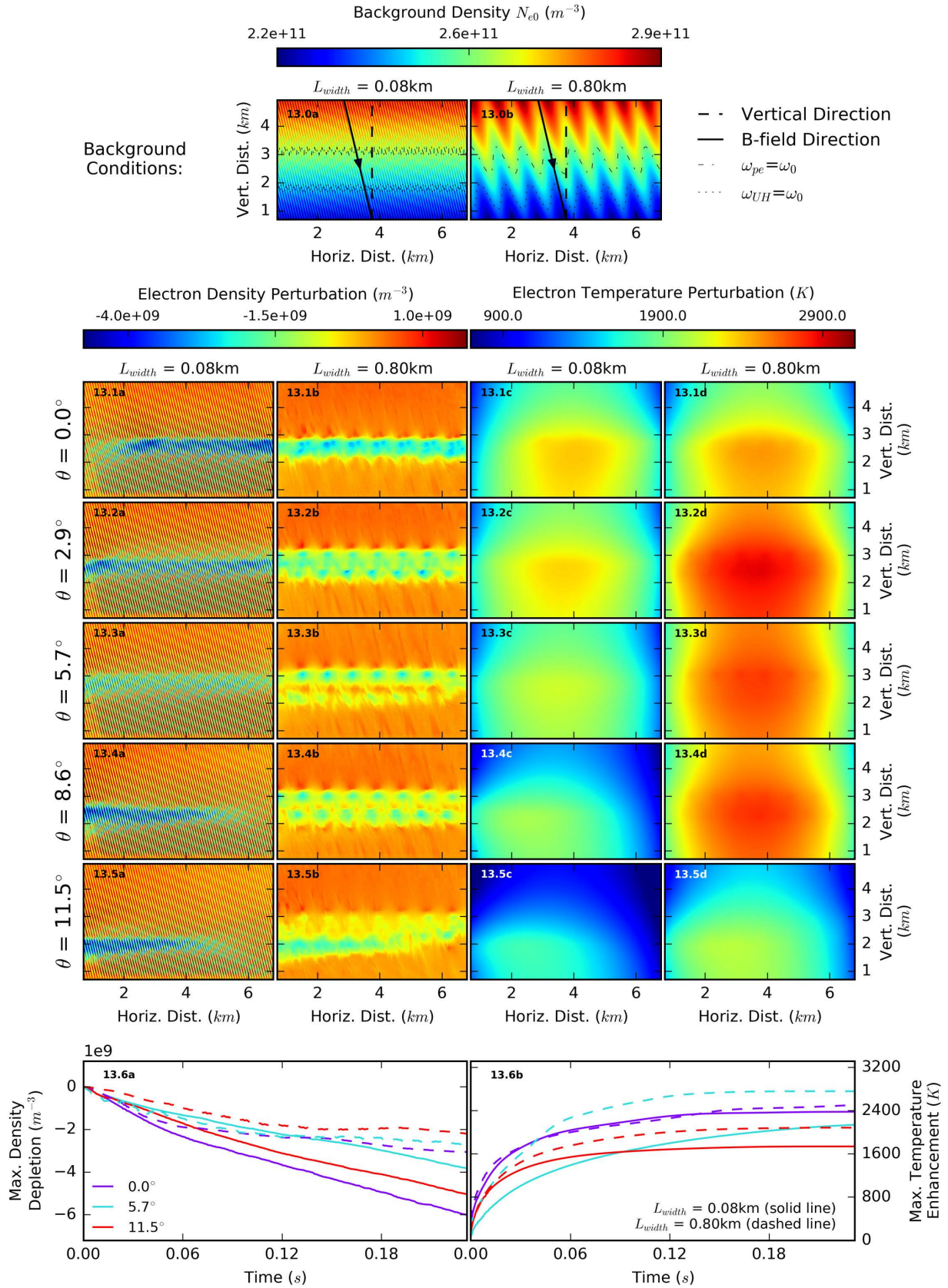


Figure 13: Variation in electron density perturbation and electron temperature perturbation with pump wave inclination angle when periodic density-depleted field-aligned irregularities of the form (11) with $L_{width} = 0.08 km$ and $L_{width} = 0.8 km$ were included in the background density profile. Uppermost panels (13.0a-b) show the background conditions for each L_{width} case. Lowermost panels (13.6a-b) show the variation of minimum density perturbation and maximum temperature perturbation recorded in the simulation with time for $L_{width} = 0.08 km$ (solid line) and $L_{width} = 0.8 km$ (dashed line).

When the single, narrow (0.08 km) irregularity was included, the simulation behaved in a similar manner to the unperturbed case, as would be expected from Figure 3 which suggests that the Z-mode window would be relatively unmodified by irregularities of this scale, with only a slight ($< 1^\circ$) shift towards vertical. In this case, the maximum temperature enhancement occurred for the pump waves directed close to the Spitze angle (5.7°) and between the Spitze and vertical directions (2.9°) consistent with the small shift in the Z-mode window. The maximum stationary-state temperature was similar to that shown for the unperturbed 1D slope case in Figure 9. At all angles, the largest density modification occurred away from the position of the density duct. For the larger-scale (0.8 km) irregularity, the temperature perturbation at all angles was greater than in the narrow-irregularity case at all sampled angles, due to the broadening of the window with increasing duct width (as shown in Figure 3). The greatest modifications to both temperature and density occurred for the wave directed between the Spitze angle and vertical (shown in panels 12.2b and 12.2d). Here, the maximum steady state temperature achieved was more than 10% greater than the maximum temperature developed in the unperturbed 1D slope scenario shown in Figure 9. At all sampled angles, the site of greatest density perturbation can be seen to occur within the duct, having the effect of deepening the depletion with time around the point at which the pump wave is reflected.

When multiple periodically-distributed irregularities were included, the growth of plasma perturbations was very different. As expected from Section 3, the smaller-scale (0.08 km) irregularities effectively attenuate the propagation of the Z-mode wave beyond the interaction region. As such, this narrow irregularity case behaves much like the unperturbed 1D density slope scenario with the effects due the Z-mode suppressed. Accordingly, the maximum temperature enhancement was found to occur for the vertically-directed pump wave (shown in panel 13.1c), and was found to decrease as the wave inclination angle was increased towards the field-aligned direction. For the larger-width (0.8 km) irregularities, as in the single-irregularity case, the greatest modification to the plasma was found to occur for the pump wave inclined at 2.9° (panel 13.2d). The greatest perturbations can be seen to be localized at certain points within each density depletion. These “hot spots” correspond to the pump wave reflection point within each irregularity (indicated in the background profile plot 13.0b). The magnitude of maximal temperature in the large-irregularity case was greater than in the small-irregularity case for all pump wave angles aside from vertical (for which the steady state temperatures were approximately equal). By contrast, the magnitude of density depletions was greater in the case of narrow irregularities by a factor of 2 or greater at all sampled angles, corresponding to a more rapid growth of the depletions with time in this scenario.

In Section 3 it was shown that addition of a 2D variation to the electron density profile strongly affected both the process of conversion from the O-mode pump wave to Z-mode and the subsequent propagation of any Z-mode waves. The results presented in this Section have demonstrated that this modification of the Z-mode window has a knock-on impact on the development of artificially-induced thermal plasma perturbations. Changing the shape or position of the Z-mode window via the inclusion of a 2-D density inhomogeneity was found to lead to a corresponding variation in the dependence of electron temperature enhancement on pump wave inclination angle. This mechanism could explain why the greatest magnitudes of plasma heating have often been found to occur for non-Spitz directed waves during observations of the magnetic zenith effect.

6. Summary and Conclusions

Ionospheric heating experiments have observed that the magnitude of artificial heating-induced plasma perturbations depend strongly on the inclination angle of the pump beam, with a greater modification to the plasma observed when the heating beam is directed close to or along the magnetic zenith direction. [Honary *et al.*, 2011] proposed that this Magnetic Zenith Effect is due to the O-mode to Z-mode conversion process that can occur in the F-region for a narrow range of pump wave inclination angles. This conversion process has previously been investigated theoretically for the case of a 1D variation in electron density, however the case of a 2D variation had not been discussed before, and in this paper was investigated numerically for the first time. A recently-developed full-wave FDTD code [Cannon and Honary, 2015] was used to numerically explore the effect of an O-mode polarized EM pump wave on the plasma around the ionosphere critical interaction region. In particular, the behaviour of the O- to Z-mode conversion process and Magnetic Zenith Effect was investigated for a variety of density profiles. These simulations shows that the presence of ionospheric plasma density inhomogeneities can explain many of the features of the observed Magnetic Zenith Effect through modification of the angular window for O-mode to Z-mode conversion.

The fraction of the simulated pump wave field penetrating beyond the O-mode reflection height in the form of a Z-mode was measured for a range of launch angles and used to determine the angular shape of the window for which O-to-Z-mode conversion was favourable. For the case of a 1D vertical electron density gradient the simulation results (as shown in Figure 1) demonstrated good agreement with the predictions of [Mjølhus, 1984], with the conversion window centred on the Spitze angle (8). From this, one would expect that the Magnetic Zenith Effect would manifest most strongly for pump waves directed at the Spitze angle, however it has been reported that

the maximum electron temperature enhancement at EISCAT can occur for inclination angles somewhere between the Spitzze and field-aligned directions (for example, [Isham *et al.*, 2005]). To explain this, [Honary *et al.*, 2011] proposed that the shape of the Z-mode window can be modified by the presence of horizontal inhomogeneities in the electron density, such as the large scale depleted regions or field-aligned irregularities that may be excited during the course of an ionospheric heating experiment. This problem cannot be fully treated theoretically using the techniques of geometric optics, however the numerical simulation techniques used here allowed 2D plasma profiles to be fully taken into account.

A varied hierarchy of electron density structures have been observed during heating experiments due to the formation of plasma irregularities of different scales. The FDTD code was used to investigate how the inclusion of 2D density inhomogeneities could influence the shape of the Z-mode window. Here three distinct cases were investigated: large-scale horizontal density slopes, medium-scale single density-depleted ducts and smaller-scale periodic field-aligned irregularities. The results demonstrate that the window is highly sensitive to the form of the density profile.

Adding a linear horizontal density gradient to represent a large-scale density-depleted patch was found to shift the centre of the Z-mode window away from the Spitzze direction, as shown in Figure 2, either towards the magnetic zenith direction or the vertical direction depending on the direction of the horizontal gradient. A steeper slope resulted in a greater shift of the window. Shifting the window all the way to the field-aligned direction required the presence of a horizontal density gradient of similar size to the vertical gradient (a similar gradient in the opposing direction would shift the window all the way to the vertical direction).

Inclusion of a single field-aligned density-depleted irregularity to represent a duct-like structure led to a slight shifting of the window towards the vertical direction for irregularities with widths $< 0.1 \text{ km}$. Increasing the irregularity width in the range $0.1 \text{ km} - 2 \text{ km}$ was found to increasingly broaden the Z-mode window, with the angular width of the window for a duct of 1 km width almost three times that of the 1D slope case (see Z-mode window curves in Figure 3). For duct widths in this range, it could be seen that a narrow Z-mode beam was produced for every sampled pump wave direction, however the location with respect to the irregularity geometry at which conversion took place varied between inclination angles, as can be seen in Figure 4. For irregularity widths beyond 2 km , this broadening effect was found to decrease, and with increasing width the shape of the Z-mode window tended towards the unperturbed form measured for the case of the 1D vertical density gradient.

Inclusion of multiple duct-like structures in the form of periodic field-aligned density-depleted irregularities had a strong effect on the propagation of the converted Z-mode (as shown in Figure 5), with transmitted waves multiply scattered by adjacent irregularities, making it difficult to measure the window shape. In general the effect of periodic irregularities with spatial scales comparable to or smaller than the pump wave wavelength had the effect of attenuating the transmitted Z-mode amplitude at all angles while maintaining the angular window shape measured for the unperturbed case. As the irregularity scale size was increased, multiple scattering of the Z-mode wave between irregularities allowed significant E-field amplitude to propagate beyond the O-mode reflection height for all sampled pump wave angles.

A novel feature of the FDTD code used here is that it allowed the time-explicit evolution of thermal perturbations to the plasma density and temperature to be simulated on the timescale of the EM wave. This feature was used to investigate how the O-mode to Z-mode conversion process may lead to an angularly-dependent modification of the plasma medium. In the F-region of the ionosphere, the Z-mode wave is reflected at a higher altitude than the O-mode wave at a point corresponding to $X = Y + 1$. If reflected, the Z-mode wave is able to propagate back towards the interaction region where it can excite a resonance that is inaccessible to fast X-mode waves and results in the efficient conversion of the EM wave to upper-hybrid plasma waves. As the Z-mode wave approaches the resonance height, its k-vector approaches infinity and thus its group velocity decreases, leading to a sharp increase in electric field amplitude. The swelling in amplitude leads to the growth of local electron temperature, thus an increase in the pressure and causing the expansion of the local plasma. To investigate the impact of this process, simulations in which the Z-mode wave was allowed to reflect back towards the interaction height were compared with simulations in which the Z-mode was absorbed before reflection using an artificial PML, both for the case of a 1D linear density variation (see Figures 7 and 8). For a Spitzze-directed wave, the maximum E-field amplitude measured when the Z-mode wave was allowed to reflect was more than 10 times greater than in the reflection-suppressed case. Correspondingly, the magnitude of thermal perturbations to the plasma were found to be greater in the reflection allowed scenario, with electron temperature enhanced by factor of 2 and electron density depleted by a factor of 4 compared to the Z-mode reflection-suppressed results.

In the reflection-allowed simulations, the angular dependence in O-to-Z-mode conversion translated to an angular dependence in plasma modification, demonstrated by the results presented in Figure 9. Pump waves with inclination angles more favourable for Z-mode conversion were found to achieve a greater magnitude of plasma perturbation, with the magnitude of steady-state temperature enhancement increasing as the wave inclination angle was increased from 2780 K at vertical (0.0°) to 2940 K at the Spitzze (5.2°), before falling off as the inclination

angle was increased further. By contrast, without Z-mode reflection the greatest electron temperature enhancement was seen for the vertically-directed (2750K) wave and the level of enhancement reduced as the inclination angle approached the Spitze (1440K). In addition, excitement of small-scale field-aligned density irregularities was found to occur most favourably for pump beams directed along the Spitze direction, as shown in Figure 10. These results support the idea that resonant excitation of large-amplitude electric fields via the reflected Z-mode contributes to the enhanced plasma perturbations and pump wave inclination angle dependence associated with the Magnetic Zenith Effect.

The addition of a horizontal component to the linear density profile was shown to modify the Z-mode window by shifting its centre away from the Spitze direction and here it was shown that this also had a significant impact on the development of thermal plasma perturbations. Simulations were run using the density profile given by (9) for horizontal slope scale sizes of 50 km and 20 km (see results presented in Figure 11). Maximum temperature enhancement found to occur for pump wave inclination angles 8.6° and 11.5° respectively, corresponding closely to the centre of the Z-mode window for each scenario (8.3° and 12.4° respectively). Thus, by shifting the Z-mode window via a horizontal density inhomogeneity, the pump wave inclination angle resulting in the greatest heating was found to vary. This offers a potential mechanism to explain how maximal Magnetic Zenith Effect heating has been observed to occur for non-Spitze directed waves.

Simulations were run to compare the influence of duct-like irregularities of large (800 m) and smaller (80 m; close to the pump wavelength) scale sizes on the growth of thermal plasma perturbations (see results presented in Figure 12). As would be expected from the simulated Z-mode window curves shown in Figure 3, the narrow irregularity case behaved much like the unperturbed case with maximum temperature enhancement occurring at the Spitze angle. For the larger irregularity, greater stationary-state temperatures were achieved at all angles due to the broadening of the Z-mode window for irregularities of this type. Both the maximum temperature enhancement and the greatest depletion of density occurred for the wave directed between the Spitze angle and vertical. For a pump wave at this angle, the stationary temperature enhancement was 10% greater than in the unperturbed 1D slope case shown in Figure 9.

For periodic irregularities of the same scale sizes, the growth of plasma perturbations was very different (as shown in Figure 13). The narrow irregularities ($L_{width}=80$ m) effectively attenuated conversion of the O-mode wave to the Z-mode, leading to the greatest plasma perturbations occurring when the pump wave was directed vertically. For the larger irregularities ($L_{width}=800$ m), as in the single-irregularity case, the greatest modification to the plasma occurred for a pump wave inclination angle of 2.9°. The greatest perturbations can be seen to occur in highly-localized hot spots within the periodic density depletions. The magnitude of temperature in the large-irregularity case was greater than in the small-irregularity case for all pump wave angles aside from vertical (for which the steady state temperatures were approximately equal). By contrast, the magnitude of density depletions were greater in the case of narrow irregularities by a factor of 2 or more at all angles, corresponding to a more rapid growth of the depletions in this scenario.

The simulations presented in this paper demonstrate that the existence of 2D electron density inhomogeneities around the O-mode reflection height can have a significant impact on the development of perturbation to the plasma during a heating experiment. Large-scale linear density gradients, medium-scale duct-like density depletions and small-scale field-aligned irregularities were all found to affect the O-mode to Z-mode conversion process and consequently modify the position of the Z-mode window. This was shown to have a knock-on effect on the growth of thermal plasma perturbations due to the interaction of the heating wave and offers a potential mechanism behind several of the observed features of the Magnetic Zenith Effect.

Acknowledgments. P. D. Cannon is supported by an STFC studentship. The simulations presented in this work were run using the Lancaster University High-End Cluster. Simulation source code and output data are available on request from the corresponding author (p.cannon@lancaster.ac.uk).

Copyright 2016 by the American Geophysical Union.
0148-0227/16/\$9.00

References

- Antani, S. N., D. J. Kaup, and N. N. Rao (1996), Excitation of upper hybrid waves from ordinary-mode electromagnetic waves via density gradient in the ionosphere, *Journal of Geophysical Research: Space Physics*, 101(A12), 27,035–27,041, doi:10.1029/96JA02634.
- Berenger, J. P. (1994), A perfectly matched layer for the absorption of electromagnetic waves, *J. Comp. Phys.*, 114, 185–200, doi:10.1006/jcph.1994.1159.
- Bilitza, D., D. Altadill, Y. Zhang, C. Mertens, V. Truhlik, P. Richards, L.-A. McKinnell, and t. . Reinisch, Bodo” (2014).
- Borisov, N., and T. Robinson (2003), Transformation of an EM pump wave into upper hybrid resonance oscillations in striations in a vertically inhomogeneous ionosphere, *Physics Letters A*, 315(12), 126 – 135, doi:10.1016/S0375-9601(03)00978-2.
- Budden, K. G. (1961), *Radio Waves in the Ionosphere*, 1st ed., Cambridge University Press, London.
- Cannon, P. D., and F. Honary (2015), A GPU-accelerated finite-difference time-domain scheme for electromagnetic wave interaction with plasma, *Antennas and Propagation, IEEE Transactions on, PP(99)*, doi:10.1109/TAP.2015.2423710.

- Cummer, S. A. (1997), An analysis of new and existing FDTD methods for isotropic cold plasma and a method for improving their accuracy, *IEEE Trans. Antennas Propag.*, *45*(3), doi:10.1109/8.558654.
- Dhillon, R. S., and T. R. Robinson (2005), Observations of time dependence and aspect sensitivity of regions of enhanced UHF backscatter associated with RF heating, *Annales Geophysicae*, *23*(1), 75–85, doi:10.5194/angeo-23-75-2005.
- Djuth, F. T., B. Thidé, H. M. Ierkic, and M. P. Sulzer (1987), Large F-region electron-temperature enhancements generated by high-power HF radio waves, *Geophysical Research Letters*, *14*(9), 953–956, doi:10.1029/GL014i009p00953.
- Dysthe, K. B., E. Mjølhus, H. Pécseli, and K. Rypdal (1982), Thermal cavitons, *Physica Scripta*, *1982*(T2B), 548, doi:10.1088/0031-8949/1982/T2B/040.
- Eliasson, B., and L. Stenflo (2008), Full-scale simulation study of the initial stage of ionospheric turbulence, *Journal of Geophysical Research: Space Physics*, *113*(A2), n/a–n/a, doi:10.1029/2007JA012837.
- Ginzburg, V. L. (1970), *The propagation of electromagnetic waves in plasmas*, 2nd ed., Pergamon Press, New York.
- Gondarenko, N. A., P. N. Guzdar, G. M. Milikh, and S. L. Ossakow (2002), Modification of the electron density profile near the upper hybrid layer during radio wave heating of the ionosphere, *Geophysical Research Letters*, *29*(11), 5–1–5–4, doi:10.1029/2002GL014934.
- Gondarenko, N. A., P. N. Guzdar, S. L. Ossakow, and P. A. Bernhardt (2003), Linear mode conversion in inhomogeneous magnetized plasmas during ionospheric modification by HF radio waves, *J. Geophys. Res.*, *108*(A12), doi:10.1029/2003JA009985..
- Gondarenko, N. A., S. L. Ossakow, and G. M. Milikh (2005), Generation and evolution of density irregularities due to self-focusing in ionospheric modifications, *J. Geophys. Res.*, *110*(A09304), doi:10.1029/2005JA011142.
- Gondarenko, N. A., S. L. Ossakow, and G. M. Milikh (2006), Nonlinear evolution of thermal self-focusing instability in ionospheric modifications at high latitudes: Aspect angle dependence, *Geophys. Res. Lett.*, *33*(L16104), doi:10.1029/2006GL025916.
- Gordon, W. E., and H. C. Carlson (1974), Arecibo heating experiments, *Radio Science*, *9*(11), 1041–1047, doi:10.1029/RS009i011p01041.
- Gurevich, A., A. Lukyanov, and K. Zybin (1995), Stationary state of isolated striations developed during ionospheric modification, *Physics Letters A*, *206*(34), 247 – 259, doi:10.1016/0375-9601(95)00595-T.
- Gurevich, A., T. Hagfors, H. Carlson, A. Karashtin, and K. Zybin (1998), Self-oscillations and bunching of striations in ionospheric modifications, *Physics Letters A*, *239*(6), 385 – 392, doi:10.1016/S0375-9601(98)00006-1.
- Gurevich, A., H. Carlson, and K. Zybin (2001), Nonlinear structuring and southward shift of a strongly heated region in ionospheric modification, *Physics Letters A*, *288*(34), 231 – 239, doi:10.1016/S0375-9601(01)00516-3.
- Gurevich, A., E. Fremouw, J. Secan, and K. Zybin (2002), Large scale structuring of plasma density perturbations in ionospheric modifications, *Physics Letters A*, *301*, 307–314, doi:10.1016/S0375-9601(02)00901-5.
- Gurevich, A., K. Zybin, and H. Carlson (2005), Magnetic-zenith effect, *Radiophysics and Quantum Electronics*, *48*(9), 686–699, doi:10.1007/s11141-005-0113-7.
- Gurevich, A. V. (1978), *Nonlinear Phenomena in the Ionosphere*, 1st ed., Springer Berlin Heidelberg.
- Honary, F., A. Stocker, T. Robinson, T. Jones, N. Wadh, P. Stubbe, and H. Kopka (1993), EISCAT observations of electron temperature oscillations due to the action of high power HF radio waves, *Journal of Atmospheric and Terrestrial Physics*, *55*(10), 1433 – 1448, doi:10.1016/0021-9169(93)90109-C.
- Honary, F., N. Borisov, M. Beharrell, and A. Senior (2011), Temporal development of the magnetic zenith effect, *Journal of Geophysical Research: Space Physics*, *116*(A6), doi:10.1029/2010JA016029.
- Isham, B., T. Hagfors, B. Z. Khudukon, Y. Yurik, E. D. Tereshchenko, M. T. Rietveld, V. Belyey, M. Grill, C. La Hoz, A. Brekke, and C. Heinselman (2005), An interferometer experiment to explore the aspect angle dependence of stimulated electromagnetic emission spectra, *Annales Geophysicae*, *23*(1), 55–74, doi:10.5194/angeo-23-55-2005.
- Kelley, M. C., T. L. Arce, J. Salowey, M. Sulzer, W. T. Armstrong, M. Carter, and L. Duncan (1995), Density depletions at the 10-m scale induced by the Arecibo heater, *Journal of Geophysical Research: Space Physics*, *100*(A9), 17,367–17,376, doi:10.1029/95JA00063.
- Kosch, M., M. T. Rietveld, T. Hagfors, and T. B. Leyser (2000), High-latitude HF-induced airglow displaced equatorwards of the pump beam, *Geophysical Research Letters*, *27*(17), 2817–2820, doi:10.1029/2000GL003754.
- Kosch, M. J., E. Mjølhus, M. Ashrafi, M. T. Rietveld, T. Yeoman, and S. Nozawa (2011), Angular dependence of pump-induced bottomside and topside ionospheric plasma turbulence at EISCAT, *Journal of Geophysical Research: Space Physics*, *116*(A3), doi:10.1029/2010JA016014.
- Leyser, T. B., and E. Nordblad (2009), Self-focused radio frequency L wave pumping of localized upper hybrid oscillations in high-latitude ionospheric plasma, *Geophysical Research Letters*, *36*(24), n/a–n/a, doi:10.1029/2009GL041438, 124105.
- Meltz, G., L. H. Holway, and N. M. Tomljanovich (1974), Ionospheric heating by powerful radio waves, *Radio Science*, *9*(11), 1049–1063, doi:10.1029/RS009i011p01049.
- Mjølhus, E. (1984), Coupling to Z mode near critical angle, *Journal of Plasma Physics*, *31*, 7–28, doi:10.1017/S0022377800001392.
- Mjølhus, E. (1990), On linear conversion in a magnetized plasma, *Radio Science*, *25*(6), 1321–1339, doi:10.1029/RS025i006p01321.
- Mjølhus, E., and T. Flå (1984), Direct access to plasma resonance in ionospheric radio experiments, *Journal of Geophysical Research: Space Physics*, *89*(A6), 3921–3928, doi:10.1029/JA089iA06p03921.
- Nordblad, E., and T. B. Leyser (2010), Ray tracing analysis of L mode pumping of the ionosphere, with implications for the magnetic zenith effect, *Annales Geophysicae*, *28*(9), 1749–1759, doi:10.5194/angeo-28-1749-2010.
- Pedersen, T. R., M. McCarrick, E. Gerken, C. Selcher, D. Sentman, H. C. Carlson, and A. Gurevich (2003), Magnetic zenith enhancement of HF radio-induced airglow production at HAARP, *Geophysical Research Letters*, *30*(4), doi:10.1029/2002GL016096.
- Rao, N. N., and D. J. Kaup (1990), Upper hybrid mode conversion and resonance excitation of Bernstein modes in ionospheric heating experiments, *Journal of Geophysical Research: Space Physics*, *95*(A10), 17,245–17,252, doi:10.1029/JA095iA10p17245.
- Rietveld, M. T., M. J. Kosch, N. F. Blagoveshchenskaya, V. A. Kornienko, T. B. Leyser, and T. K. Yeoman (2003), Ionospheric electron heating, optical emissions, and striations induced by powerful HF radio waves at high latitudes: Aspect angle dependence, *Journal of Geophysical Research: Space Physics*, *108*(A4), doi:10.1029/2002JA009543.
- Robinson, T. R. (1989), The heating of the high-latitude ionosphere by high-power radio waves, *Phys. Reports*, *79*(2-3), 79–209, doi:10.1016/0370-1573(89)90005-7.
- Schneider, J. (2004), Plane waves in FDTD simulations and a nearly perfect total-field/scattered-field boundary, *Antennas and Propagation, IEEE Transactions on*, *52*(12), 3280–3287, doi:10.1109/TAP.2004.836403.
- Stocker, A., F. Honary, T. Robinson, T. Jones, P. Stubbe, and H. Kopka (1992), EISCAT observations of large scale electron temperature and electron density perturbations caused by high power HF radio waves, *Journal of Atmospheric and Terrestrial Physics*, *54*(1112), 1555 – 1572, doi:10.1016/0021-9169(92)90163-F.
- Stubbe, P., A. J. Stocker, F. Honary, T. R. Robinson, and T. B. Jones (1994), Stimulated electromagnetic emissions and anomalous HF wave absorption near electron gyroharmonics, *Journal of Geophysical Research: Space Physics*, *99*(A4), 6233–6246, doi:10.1029/94JA00023.
- Taflove, A., and S. C. Hagness (2000), *Computational Electrodynamics*, 2nd ed., Artech House, Boston, MA.

- Wong, A. Y., G. J. Morales, D. Eggleston, J. Santoru, and R. Behnke (1981), Rapid conversion of electromagnetic waves to electrostatic waves in the ionosphere, *Phys. Rev. Lett.*, *47*, 1340–1343, doi:10.1103/PhysRevLett.47.1340.
- Yee, K. S. (1966), Numerical solution of initial boundary value problems involving Maxwell's equations in isotropic media, *IEEE Trans. Antennas Propag.*, *14*, 302–307, doi:10.1109/TAP.1966.1138693.
- Young, J. L. (1994), A full finite difference time domain implementation for radio wave propagation in a plasma, *Radio Sci.*, *29*(6), 1513–1522, doi:10.1029/94RS01921.
- Yu, Y., and J. J. Simpson (2010), An E-J collocated 3-D FDTD model of electromagnetic wave propagation in magnetized cold plasma, *IEEE Trans. Antennas Propag.*, *58*(2), 469–478, doi:10.1109/TAP.2009.2037706.
-